Geophys. J. Int. (2005) **162,** 406–424 doi: 10.1111/j.1365-246X.2005.02579.x

Can observations of earthquake scaling constrain slip weakening?

Rachel E. Abercrombie[1] and James R. Rice[2]

[1]*Department of Earth Sciences, Boston University, Boston,* MA 02215 *USA. E-mail: rea@bu.edu*
[2]*Department of Earth and Planetary Sciences and Division of Engineering and Applied Sciences, Harvard University, Cambridge,* MA 02138 *USA*

Accepted 2004 December 23. Received 2004 November 30; in original form 2003 August 29

SUMMARY

We use observations of earthquake source parameters over a wide magnitude range ($M_W \sim$ 0–7) to place constraints on constitutive fault weakening. The data suggest a scale dependence of apparent stress and stress drop; both may increase slightly with earthquake size. We show that this scale dependence need not imply any difference in fault zone properties for different sized earthquakes. We select 30 earthquakes well-recorded at 2.5 km depth at Cajon Pass, California. We use individual and empirical Green's function spectral analysis to improve the resolution of source parameters, including static stress drop ($\Delta\sigma$) and total slip (S). We also measure radiated energy E_S. We compare the Cajon Pass results with those from larger California earthquakes including aftershocks of the 1994 Northridge earthquake and confirm the results of Abercrombie (1995): $\mu E_S/M_0 \ll \Delta\sigma$ (where μ = rigidity) and both E_S/M_0 and $\Delta\sigma$ increase as M_0 (and S) increases. Uncertainties remain large due to model assumptions and variations between possible models, and earthquake scale independence is possible within the resolution. Assuming that the average trends are real, we define a quantity $G' = (\Delta\sigma - 2\mu E_S/M_0)S/2$ which is the total energy dissipation in friction and fracture minus $\sigma_1 S$, where σ_1 is the final static stress. If $\sigma_1 = \sigma_d$, the dynamic shear strength during the last increments of seismic slip, then $G' = G$, the fracture energy in a slip-weakening interpretation of dissipation. We find that G' increases with S, from $\sim 10^3$ J m^{-2} at $S = 1$ mm ($M1$ earthquakes) to 10^6–10^7 J m^{-2} at $S = 1$ m ($M6$). We tentatively interpret these results within slip-weakening theory, assuming $G' \approx G$. We consider the common assumption of a linear decrease of strength from the yield stress (σ_p) with slip (s), up to a slip D_c. In this case, if either D_c, or more generally $(\sigma_p - \sigma_d)\, D_c$, increases with the final slip S we can match the observations, but this implies the unlikely result that the early weakening behaviour of the fault depends on the ultimate slip that the fault will sustain. We also find that a single slip-weakening function $\sigma_F(s)$ is able to match the observations, requiring no such correlation. Fitting G' over $S = 0.2$ mm to 0.2 m with $G' \propto S^{1+n}$, we find $n \sim 0.3$, implying a strength drop from peak $\sigma_p - \sigma_F(S) \propto S^n$. This model also implies that slip weakening continues beyond the final slip S of typical earthquakes smaller than $\sim M6$, and that the total strength drop $\sigma_p - \sigma_d$ for large earthquakes is typically >20 MPa, larger than $\Delta\sigma$. The latter suggests that on average a fault is initially stressed below the peak strength, requiring stress concentration at the rupture front to propagate slipping.

Key words: earthquake source parameters, fracture energy, seismic energy, slip-weakening, source scaling, stress drop.

1 INTRODUCTION

Our knowledge of the dynamics of earthquake rupture is based largely on measurements providing earthquake source parameters such as radiated seismic energy and stress drop. The scaling of these parameters over a wide range of earthquake sizes has been used to investigate the self-similarity of the earthquake rupture process and the manner in which earthquakes nucleate and grow. For example, Ohnaka (2003) compared laboratory measurements of slip with earthquake observations over a wide range of scales and argued that roughness properties in the fault zone govern the nucleation and subsequent rupture size of earthquakes. It has long been known that earthquake stress drop is relatively constant for earthquakes larger than $\sim M3$ (e.g. Hanks 1977). Abercrombie & Leary (1993) and Abercrombie (1995) used earthquake seismograms recorded at 2.5 km depth in a granite batholith, and thus unaffected by strong near-surface attenuation, to show that this roughly constant stress drop scaling continues at least to M_W 0 (Fig. 1a), although it may be argued that there is some slight trend of increasing stress drop with size for the smaller earthquakes.

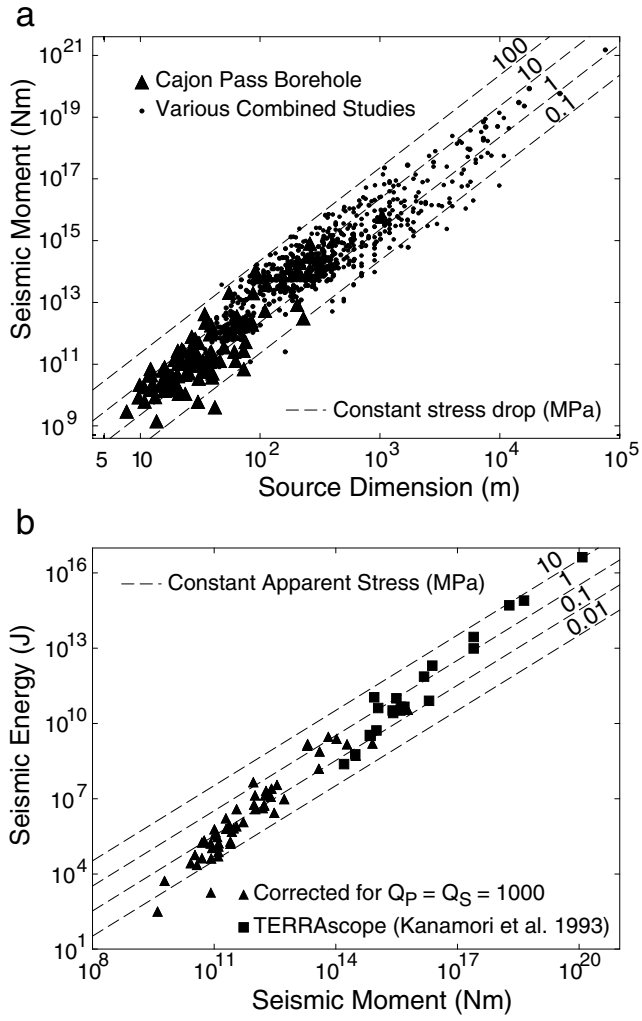

Figure 1. Earthquake scaling relationships after Abercrombie (1995): (a) source dimension, seismic moment and stress drop and (b) radiated seismic energy, seismic moment and apparent stress. The results from Abercrombie's Model 2, assuming $Q_P = Q_S = 1000$.

Abercrombie (1995) also estimated radiated seismic energy (E_S) using borehole seismograms, and found that the apparent stress

$$\sigma_a = \mu \frac{E_S}{M_0}, \tag{1}$$

where μ is the rigidity and M_0 the seismic moment (Wyss 1970), appears to increase with M_0 (Fig. 1b). Kanamori *et al.* (1993) and Mayeda & Walter (1996) obtained a similar trend for larger earthquakes in the western United States. These results imply either that the earthquake rupture process is scale dependent, and not self-similar as had previously been thought, or that the estimates of E_S are in error or biased in some way. Subsequent borehole and mining studies (e.g. Prejean & Ellsworth 2001; Richardson & Jordan 2002; Stork & Ito 2004) have confirmed a decrease in average σ_a with M_0. This trend has been interpreted as a difference in frictional behaviour during rupture between large and small earthquakes (Kanamori & Heaton 2000), or even within a single earthquake in the case of the 1999 Chi-Chi earthquake where extremely high-slip, relatively smooth rupture was observed in the northern part of the rupture area (Ma *et al.* 2001). Such a scale dependence to earthquake rupture dynamics is also consistent with studies of strong ground motion records of large earthquakes. For example, Ide & Takeo (1997) and Bouchon *et al.* (1998) estimated relatively large values for the critical breakdown slip (D_c), of the order of 1 m, for the 1995 Kobe earthquake. This is a significant fraction of the total slip in the earthquake, and much larger than the total slip of smaller earthquakes. If D_c is a property of the fault zone, then such large values of D_c would preclude the occurrence of smaller earthquakes on these faults. Thus these results suggest that the value of D_c may scale with the total slip in the earthquake. Guatteri & Spudich (2000) investigated the resolution of these studies, and showed that there is a strong trade-off between estimates of D_c and of strength excess ($= \sigma_p - \sigma_0$, where σ_p is the yield stress and σ_0 the initial stress at each point on the fault). They concluded that only the estimates of fracture energy, $G \propto (\sigma_p - \sigma_0)\, D_c$, are reliable. More recently, Ide (2002) used slip models to calculate G and D_c for three earthquakes M_W 5–7. He also found that the fracture energy ($\sim$MJ m^{-2}) is better constrained than his estimated D_c values (of $\sim$40 cm). Mikumo *et al.* (2001) and Olsen *et al.* (2001) proposed a method of obtaining D_c independent of the fracture energy, and obtained values of 30–40 cm for the western Tottori earthquake (2000). It is still unclear, however, whether the low-pass filters used to model large earthquakes (typically >1 or 2 s) preclude resolution of smaller values of D_c (e.g. Ide 2002; Guatteri & Spudich 2000).

In contrast to these suggestions of scale dependence to the earthquake rupture process, McGarr (1999) noted that the observations of maximum σ_a are constant over 14 orders of M_0. He proposed that the average values in each data set are lower because of band-limited recording. Ide & Beroza (2001) investigated the effects of band-limited recording on a range of data sets, including those of Abercrombie (1995) and Kanamori *et al.* (1993), and found that it led to significant selection bias. Ide & Beroza (2001) concluded that σ_a is constant from $\sim M_W$ 0.5 (or less) to 8, but they noted that the selection bias does not remove the entire observed trend in the range M_W 1–6. In addition, they used teleseismic estimates of E_S for a global data set of large earthquakes, with a very wide range in σ_a. Teleseismic measurements can be as much as an order of magnitude smaller than regional estimates (e.g. Singh & Ordaz 1994), and there is considerable ongoing debate as to which are most accurate (e.g. Kanamori *et al.* 1993; Choy & Boatwright 1995; Pérez-Campos & Beroza 2001; Boatwright *et al.* 2002). Also, Venkataraman & Kanamori (2004) show that σ_a varies systematically with tectonic setting, adding further uncertainties to such wide comparisons as that of Ide & Beroza (2001). Ide *et al.* (2003) reanalysed some of the small earthquakes studied by Prejean & Ellsworth (2001), using a multiple empirical Green's function (EGF) method. They concluded that simple spectral fitting (used by Prejean & Ellsworth 2001 and in most other small earthquake studies) may not be reliable even for recordings in deep boreholes. Ide *et al.* (2003) observed σ_a and $\Delta\sigma$ to be well correlated within their data set, and found no evidence for any breakdown in constant stress drop. In view of the ongoing debate, it is timely to revisit the seismograms recorded in the Cajon Pass borehole. These remain some of the least attenuated small earthquake recordings available. We use an improved technique to estimate E_S that is not affected by the selection bias. We also identify clusters of similar, closely located earthquakes, and use individual and EGF methods to obtain alternative source parameter estimates. We then combine our results with those of previous studies over a wide scale range and investigate what constraints they can place on the dynamic earthquake rupture process. We begin with a review of the energy budget of earthquake rupture and some of the models of dynamic rupture currently in use.

2 THE EARTHQUAKE ENERGY BUDGET AND MODELS OF DYNAMIC RUPTURE

Kanamori & Heaton (2000) provide a summary of the energy budget of earthquake rupture, which we follow here. We consider the energy budget of each subfault or patch of fault as the rupture front passes. An earthquake is viewed as a stress release process on a surface of area A. In the simplest case (Fig. 2a), at the start of an earthquake the resisting stress on the fault plane (σ_F, thick black line) drops from the initial (before an earthquake) shear stress (σ_0) to a constant dynamic friction level equal to the final dynamic stress, σ_d. If the condition for instability is satisfied, rapid fault slip motion begins and eventually stops. At the end of the earthquake, the stress on the fault plane is σ_1 (final static stress), and the average slip (or displacement) is S. Hence $\sigma_F(S) = \sigma_d$, and in the simple case shown in Fig. 2(a), $\sigma_d = \sigma_1$. The static stress drop $\Delta\sigma = \sigma_0 - \sigma_1$. During this process, the potential energy (strain energy plus gravitational energy) of the system, W, drops by ΔW, which can be written as

$$\Delta W = E_S + FA + GA$$

where F is the frictional energy loss per unit area, given by $F = \sigma_d S$, E_S is the energy radiated as seismic waves, and G is the fracture energy per unit area (essentially, G accounts for all dissipation in excess of the dissipation $\sigma_d S$ per unit area identified above as F). Knopoff (1958), Kostrov (1974) and Dahlen (1977) commented that $\Delta W = \bar{\sigma} A S$, where $\bar{\sigma} = (\sigma_0 + \sigma_1)/2$ is the average of the static stresses before and after faulting. The energy balance is easily interpreted in the simplest case shown in Fig. 2(a), often referred to as the Orowan model (Orowan 1960). In this simple model the fracture energy is negligible ($G = 0$), and so

$$\frac{E_S}{A} = \frac{\Delta\sigma}{2} S,$$

and the apparent stress, $\sigma_a = \Delta\sigma/2$. In this model, if earthquakes have a constant stress drop, then they would also have a constant σ_a and thus the model is scale-invariant. The variation in resisting stress during rupture, $\sigma_F(s)$, is likely to be considerably more complex than is shown in Fig. 2(a). Laboratory experiments, numerical models and seismic inversion studies predict changes in stress at each point on the rupture surface during the rupture before, during and after the slip at that individual point. Fig. 2(b) demonstrates examples of this more complex behaviour. For example, elementary elastic and fracture mechanics considerations require that the advancing rupture front causes an increase in stress prior to dynamic slip. Such an increase is inferred, if not well resolved, in seismological inversion studies of well-recorded, large earthquakes (e.g. Miyatake 1992; Beroza & Mikumo 1996; Ide & Takeo 1997; Bouchon *et al.* 1998). We refer to the peak stress reached at the onset of dynamic slip as σ_p (see Fig. 2b); $\sigma_p - \sigma_0$ is known as the strength excess.

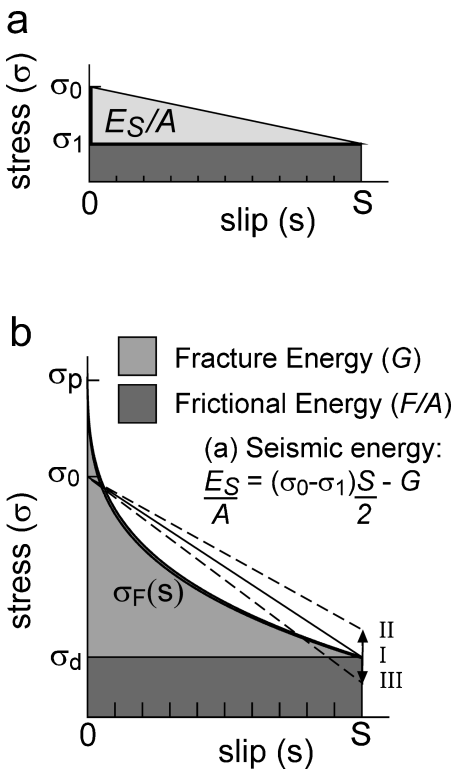

Figure 2. Model of earthquake rupture to define terms used in this paper. (a) Simple case, in which the fracture energy, $G = 0$, and the resisting stress (σ_F) falls instantaneously to $\sigma_d = \sigma_1$. (b) More general case. The approaching rupture front causes stress to rise from an initial value of σ_0 to the peak stress, σ_p. The resisting stress (thick black line, σ_F) falls to the final dynamic value, σ_d, as slip, s, increases to a final value, S. In Case I, the final static stress equals the final dynamic stress ($\sigma_d = \sigma_1$), and the seismic energy is given in the figure. In Case II the final static stress is larger, and in Case III smaller, than the final dynamic stress, representing the undershoot (partial stress, $\sigma_d < \sigma_1$) and overshoot ($\sigma_d > \sigma_1$) models respectively. In Case II the radiated seismic energy (E_S) is larger than in Case I, and in Case III E_S is smaller than in Case I.

Knopoff (1958), Kostrov (1974) and Dahlen (1977) commented that $\Delta W = \bar{\sigma} A S$, where $\bar{\sigma} = (\sigma_0 + \sigma_1)/2$ is the average of the static stresses before and after faulting. The energy balance is easily interpreted in the simplest case shown in Fig. 2(a), often referred to as the Orowan model (Orowan 1960). In this simple model the fracture energy is negligible ($G = 0$), and so

$$\frac{E_S}{A} = \frac{\Delta\sigma}{2} S,$$

and the apparent stress, $\sigma_a = \Delta\sigma/2$. In this model, if earthquakes have a constant stress drop, then they would also have a constant σ_a and thus the model is scale-invariant. The variation in resisting stress during rupture, $\sigma_F(s)$, is likely to be considerably more complex than is shown in Fig. 2(a). Laboratory experiments, numerical models and seismic inversion studies predict changes in stress at each point on the rupture surface during the rupture before, during and after the slip at that individual point. Fig. 2(b) demonstrates examples of this more complex behaviour. For example, elementary elastic and fracture mechanics considerations require that the advancing rupture front causes an increase in stress prior to dynamic slip. Such an increase is inferred, if not well resolved, in seismological inversion studies of well-recorded, large earthquakes (e.g. Miyatake 1992; Beroza & Mikumo 1996; Ide & Takeo 1997; Bouchon *et al.* 1998). We refer to the peak stress reached at the onset of dynamic slip as σ_p (see Fig. 2b); $\sigma_p - \sigma_0$ is known as the strength excess.

As slip stops at a point, the stress there in the last moments of slip equals what we call here the dynamic friction stress σ_d; thus, $\sigma_d = \sigma_F(S)$. However, after cessation of slip at this point, the passage of dynamic stress waves and slip at other locations could cause the final static stress (σ_1) to differ from σ_d, i.e. from $\sigma_F(S)$. In case (I), Fig. 2(b), friction decreases during the seismic slip, from σ_p to a final static stress $\sigma_1 = \sigma_d = \sigma_F(S)$. In cases (II) and (III), Fig. 2(b), the stress changes after the point has finished slipping result in slip undershoot ($\sigma_1 > \sigma_d$, i.e. partial stress drop) or overshoot ($\sigma_d > \sigma_1$), respectively, relative to the slip expected under the dynamic stress drop $\sigma_0 - \sigma_d$. Dynamic rupture models including a propagating slip pulse predict (at least in 2-D modelling of steady propagation) only partial stress drop (or undershoot), so that the final stress is higher than the lowest frictional stress (Heaton 1990; Perrin *et al.* 1995). Overshoot, however, is a common prediction from classical singular crack models or slip-weakening models with a constant, rate-independent, friction strength that is approached at sufficiently large slip. At least that is so for models in which the propagating rupture fronts are stopped at barriers that are roughly equidistant from the nucleation site. Madariaga (1976) found in such cases that $\sigma_d - \sigma_1 = 0.15$–$0.20$ $(\sigma_0 - \sigma_d)$, which means an overshoot $\sigma_d - \sigma_1 = 0.13$–$0.17\,\Delta\sigma$. Nevertheless, nucleating the rupture near a barrier in such crack or slip-weakening models can lead to an arrest phase which propagates towards the opposite, still propagating, edge of the rupture (Day 1982; Johnson 1990), forming a self-healing pulse configuration. That might instead lead to undershoot, although general rules on whether there is overshoot or undershoot are not yet well established for such cases.

In much of the following analysis and discussion we consider only the simpler case where there is no overshoot or undershoot, and $\sigma_d = \sigma_F(S) = \sigma_1$. We address the effect of a non-negligible difference between and σ_d and σ_1 in Section 5.

Of course, the stresses and slip discussed are not uniform on a fault, and to make use of seismic observations as we do we must deal with their averages over the rupture during each event. Our

focus is on how these parameters vary with one another over a broad range, e.g. S from millimetres to metres, and we will take the averages for individual earthquakes as being possibly representative of an approximately universal relation between strength and slip. For example, if for earthquakes A, B, C, ... we infer average parameters σ_{dA}, σ_{dB}, σ_{dC}, ... and S_A, S_B, S_C, ... , then we will think of such values defining a function $\sigma_d = \sigma_F(S)$ which we then assume to describe, approximately, how strength varies with slip at representative points on any of the faults considered.

A large number of laboratory experiments have been designed to understand the changes in the frictional stress at a point during the seismic slip. Some of these can be interpreted in a slip-weakening context, with friction decreasing as a function of slip, $\sigma = \sigma_F(s)$ (Rice 1980; Wong 1982, 1986; Ohnaka 1996). A more precise viewpoint is that friction can be an increasing function of slip rate and of the age, hence strength, of the contacting friction asperities. The latter component of strength is commonly represented by a state variable (Ruina 1983; Marone 1998). The asperity ages are shorter under rapid slip so that net rate weakening, hence potentially unstable slip, can result (Dieterich 1979, 1981; Dieterich & Kilgore 1994). The resulting framework of rate- and state-dependent friction, with temperature-dependent constitutive parameters (e.g. Blanpied *et al.* 1995) that control rate weakening or rate strengthening, can produce the primary phenomenology of crustal earthquakes (Tse & Rice 1986; Rice & Ben-Zion 1996; Scholz 1998; Lapusta & Rice 2003). When predictions within that framework are examined at the tip of a rapidly propagating rupture (Cocco & Bizzarri 2002), the response is similar in form to the predictions of the simpler slip-weakening model, with $\sigma = \sigma_F(s)$, that we adopt in our discussion here. Such coincidence with a slip-weakening model is also predicted when shearing occurs under conditions that are too rapid for escape of heat or pore fluids and weakening results from thermal pressurization of the fluid (Lachenbruch 1980; Mase & Smith 1987).

Fig. 3 shows a range of models that have been proposed to describe the earthquake rupture process. The laboratory studies of frictional slip have demonstrated that the frictional resisting stress (σ_F) does not fall instantaneously but gradually during initial slip. Working within the slip-weakening description of that fall-off, we define the fracture energy per unit area as a function of increasing slip (s) in the earthquake as (Ida 1972; Palmer & Rice 1973)

$$G = \int_0^S (\sigma_F(s) - \sigma_d)\, ds \tag{2}$$

with $\sigma_d = \sigma_F(S)$. Strictly, Palmer & Rice (1973) and Rice (1980) showed that the expression in (2) coincided with the fracture energy, G, of singular crack mechanics in circumstances for which the slip-weakening process was complete, in the sense that $\sigma_F(s)$ had reduced to a constant level σ_d, at a slip s that was much less than the total slip S in the earthquake. Here we wish to consider also cases such as that illustrated schematically in Fig. 2(b) for which the weakening process is not fully completed even at the total slip S of the earthquake.

This decrease in frictional stress is often considered to occur over a critical distance referred to as D_c. In such a model, D_c can either be a constant, at least for a given fault or region (Fig. 3a) or might be considered to be scale dependent (Ohnaka 1996), increasing with earthquake size (Fig. 3b). In these models,

$$G = \frac{\sigma_p - \sigma_d}{2} D_c. \tag{3}$$

In the former case, at scales where $S \gg D_c$, σ_a will be constant. In the latter case, the rupture process is clearly scale dependent and

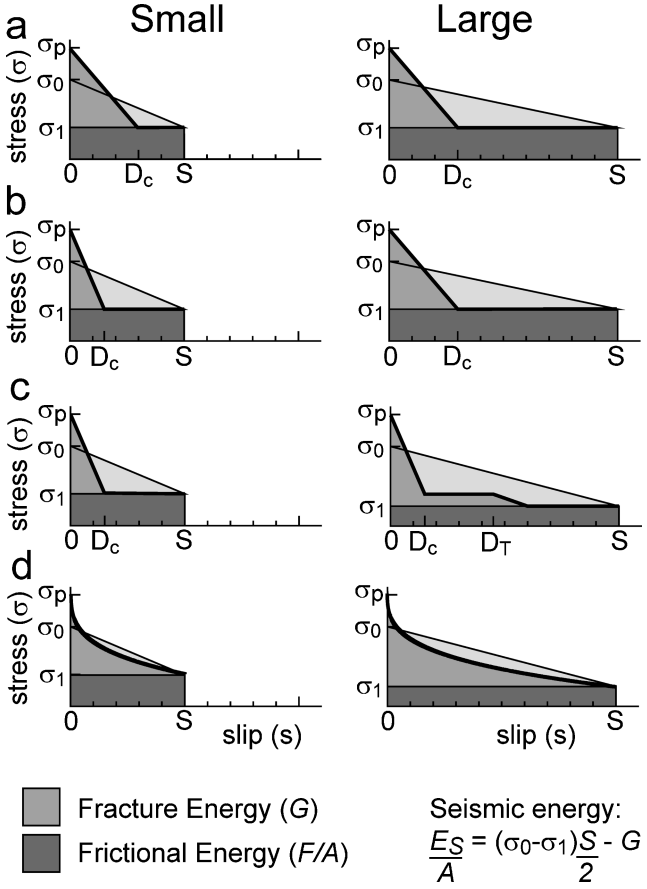

Figure 3. Models of earthquake rupture comparing large and small earthquakes—see text for description. The approaching rupture front causes stress to rise from an initial value of σ_0 to the peak stress, σ_p. Stress then falls to the final value, σ_1, as slip, s, increases to a final value, S. The thick black line is the resisting stress, σ_F: (a) constant fracture energy and D_c; (b) fracture energy and D_c increase with increasing earthquake size and slip; (c) fault lubrication, after Kanamori & Heaton (2000), friction drops initially to σ_T, but then at large slips decreases further; and (d) resisting friction stress is a function of slip, but is independent of earthquake size. Model (a) is scale independent and model (b) implies a relationship between the fault parameters (e.g. D_c), and the magnitude of slip.

there is a relationship between D_c and the size of the earthquake. Thus, if D_c is interpreted as a property of the fault zone, then it would imply that the slip at any point on a fault, and hence the magnitude of an earthquake on any given patch of fault, is governed by the D_c value at that location. Also, assuming that $\Delta\sigma$ is constant, it implies that if we could measure either D_c or the initial rate of decrease in frictional stress we could predict the size of the subsequent earthquake. Ohnaka (1996, 2003) developed such a model, using laboratory and seismological data, and argued that it is consistent with the various observations. He proposed that it is the fault surface roughness that controls D_c, and hence the amount of slip in an earthquake. There are a number of problems with this kind of model, however, including the observations that the largest slip is often not situated at the hypocentre—for example, the 1992 Landers earthquake (Wald & Heaton 1994) and the 1999 Chi-Chi earthquake (Ma *et al.* 2001).

Kanamori & Heaton (2000) proposed an alternative model that could match the observations in Fig. 1. Their model involves a constant D_c, and hence initial fracture energy, but at large slips (D_T) there is a second drop in frictional stress (Fig. 3c). Similar

concepts were introduced by Rice (1996) who argued that the rate- and state-dependent friction of Dieterich (1981) and Ruina (1983) would provide a weakening process active for the small, multimicrometre-scale, slips at which earthquakes nucleate but that additional thermal weakening by the pore fluid mechanism of Lachenbruch (1980) and Mase & Smith (1987) would take place at larger slips in the range of a few tens of millimetres. Small earthquakes will never experience the latter and so have relatively low radiated energy compared with larger earthquakes in which a significant amount of slip happens at the lower frictional stress (σ_T). Such a model as envisioned by Kanamori & Heaton (2000) would predict a step change in σ_a at D_T but would be able to fit the gradual change observed (Fig. 1) if D_T varies considerably from earthquake to earthquake or if the thermal weakening sets in gradually. Thermal weakening could also result from melting and has been speculated (Brodsky & Kanamori 2001; Ma *et al.* 2001, 2003) to involve elastohydrodynamic lubrication. Such weakening may provide an explanation for the large but smooth slip in the northern part of the rupture zone of the 1999 Chi-Chi earthquake (Ma *et al.* 2001).

If $\Delta\sigma$ and σ_a are constant, within uncertainties, the model shown in Fig. 3(a) is possible, and the earthquake rupture process can be considered scale-invariant. If, however, the relationships shown in Fig. 1 prove reliable, then we must consider whether the fault properties govern the rupture, independent of the stress conditions (Fig. 3b), whether the earthquake rupture process is essentially bimodal (Fig. 3c) or whether there is some other option. For example, we show in Fig. 3(d) a possible model in which the frictional stress decreases with increasing slip in the same manner, independent of the earthquake size or location, but the fracture energy increases with earthquake size. In this model, as in Fig. 3(c), the $\Delta\sigma$ must also increase with earthquake size. As noted by Kanamori & Heaton (2000), a small increase in $\Delta\sigma$ can lead to a large difference in radiated energy, and we investigate whether such a model is consistent with the data.

3 DATA AND ANALYSIS

3.1 Data selection

First we select 18 earthquakes from the 115 used by Abercrombie (1995), using stricter criteria including high signal-to-noise ratio and proximity to the borehole. All earthquakes were within 15 km of the borehole, and were recorded by the instrument at 2.5 km depth (Abercrombie 1995; Manov *et al.* 1996), on three components at sample rates of 500 or 1000 samples per second. We then search the complete catalogue recorded at 2.5 km for earthquakes with waveforms very similar to those of the 18 selected earthquakes, in order to identify clustered earthquakes and enable the use of empirical Green's function techniques in the subsequent analysis. We find 12 further earthquakes that meet our selection criteria. Thus in total we have 30 earthquakes (Table 1) of which 26 are part of seven clusters (termed 1A, 1B, 1C, 1E, 2C, 4C, 8A) each with two to five members. The earthquakes in a cluster have *S*–*P* times typically within 1 ms (largest variation is 5 ms), and similar waveforms

Table 1. Hypocentral parameters for the earthquakes recorded at Cajon Pass. The relocations by Hauksson (2000) are given for earthquakes recorded by the SCSN. Earthquakes with $M_L = 0$ were not recorded by the SCSN. If they are part of a cluster then the location of the largest earthquake in the cluster is given.

ID	Cluster	Year	JDay	Trigg	Hr	Min	Sec	M_L	Lat. (°)	Long. (°W)	Depth (km)	Dist. (km)
02	2C	1993	138	9	17	9	5.77	3.7	34.2937	117.4807	12.75	10.00
03	1A	1992	106	20	19	5	47.31	3.4	34.2912	117.5653	5.81	9.16
04	—	1992	113	4	6	36	46.70	2.8	34.2327	117.4338	13.56	14.02
05	1B	1992	173	18	19	1	10.37	2.5	34.2643	117.5288	8.42	9.42
07	8A	1992	261	27	0	0	0	2.2	34.2305	117.5327	8.80	12.11
08	—	1993	186	5	20	8	57.74	2.0	34.2373	117.4782	9.55	11.06
09	1B	1992	173	20	19	13	51.11	1.9	34.2648	117.5295	8.40	9.38
10	4C	1993	131	2	4	52	21.31	1.8	34.2082	117.5262	5.43	13.80
11	1E	1993	134	4	10	36	35.04	1.8	34.2937	117.4743	12.78	9.43
12	3B	1992	150	2	2	9	58.07	1.8	34.2087	117.5098	6.21	12.94
13	—	1992	108	6	5	14	34.50	1.7	34.2187	117.4220	11.72	14.69
14	—	1992	134	17	10	22	9.57	1.7	34.2492	117.4755	11.07	10.09
15	4C	1993	151	11	21	46	27.91	1.7	34.2072	117.5223	6.02	14.24
16	—	1992	334	42	16	29	21.51	1.5	34.2303	117.4670	12.60	13.16
17	1C	1992	174	3	6	59	52.71	1.3	34.2607	117.5228	9.85	9.38
18	2C	1993	44	9	2	57	37.32	1.3	34.2748	117.4555	13.62	10.07
19	8A	1992	263	6	2	24	42.79	1.2	34.2305	117.5327	8.80	12.11
20	—	1993	178	6	12	20	45.00	1.1	34.2957	117.4818	11.76	7.93
21	1C	1992	108	10	0	0	0	0	34.2607	117.5228	9.85	9.40
22	1C	1992	173	19	0	0	0	0	34.2607	117.5228	9.85	9.35
23	1C	1992	173	21	0	0	0	0	34.2607	117.5228	9.85	9.38
24	2C	1993	43	11	0	0	0	0	34.2748	117.4555	13.62	10.02
25	2C	1993	43	13	0	0	0	0	34.2748	117.4555	13.62	10.00
27	2C	1993	46	3	0	0	0	0	34.2748	117.4555	13.62	10.01
28	1E	1993	69	6	0	0	0	0	34.2937	117.4743	12.78	9.42
29	1E	1993	134	3	0	0	0	0	34.2937	117.4743	12.78	9.39
30	1E	1993	134	5	0	0	0	0	34.2937	117.4743	12.78	9.34
31	1E	1993	136	12	0	0	0	0	34.2937	117.4743	12.78	9.44
32	1A	1992	106	21	0	0	0	0	34.2912	117.5653	5.81	9.25
33	1A	1992	106	23	0	0	0	0	34.2912	117.5653	5.81	9.16

Jday, the Julian day.
Trigg, the trigger number at Cajon Pass that day.
Dist., hypocentral distance from borehole station, from the *S*–*P* phase arrival times.

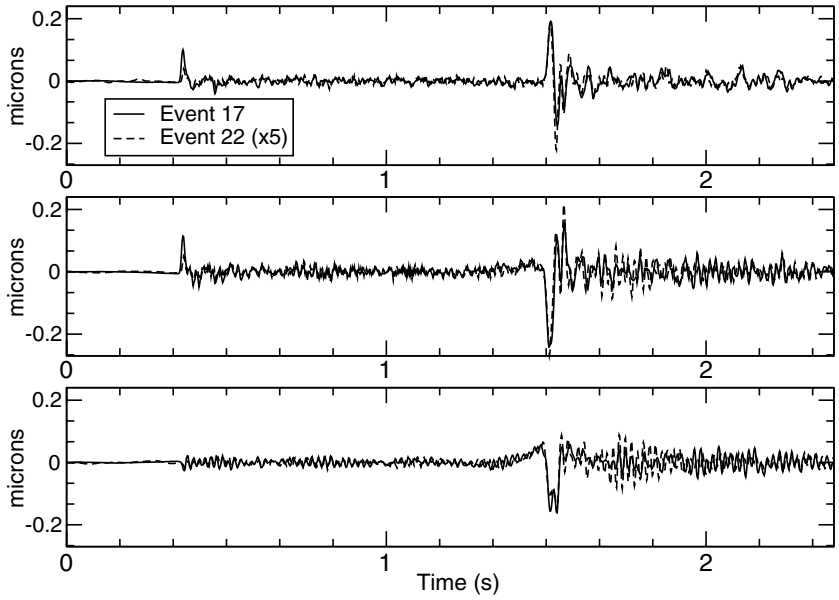

Figure 4. Three-component seismograms deconvolved to displacement for two closely located earthquakes, 17 (solid) and 22 (dashed) in Cluster 1C. The amplitudes of the smaller earthquake (22) are all multiplied by 5. Note the similarities on all components.

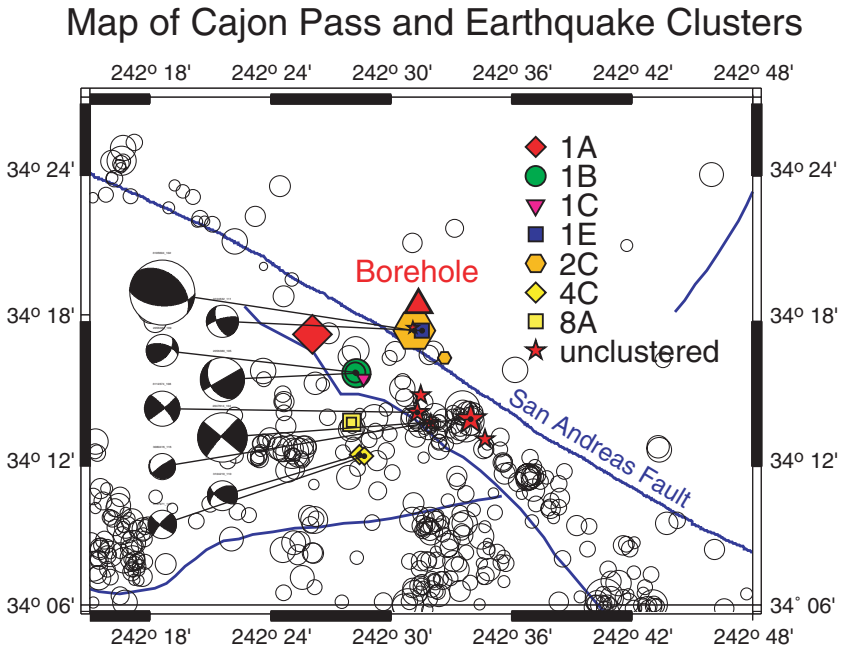

Figure 5. Map showing the location of the Cajon Pass borehole, the earthquakes considered here that are large enough to have been located by the SCSN (symbol key on map), and the SCSN-located earthquakes from 1992–1994 (open circles). Focal mechanisms (Hauksson 2000) are plotted where available.

including P and S polarity and amplitude ratio on all three components (Fig. 4). They therefore must be closely located and have similar focal mechanisms. Of the 30 earthquakes, 18 were large enough to be recorded by the Southern California Seismic Network (SCSN), and they are plotted in Fig. 5.

3.2 Spectral fitting

We calculate P and S wave displacement spectra (f) using 1 s time windows, and then model them using

$$\Omega(f) = \frac{\Omega_0 \exp(-\pi f t/Q)}{[1 + (f/f_c)^{2n}]^{0.5}}$$

where Ω_0 is the long-period level, t is the traveltime, f is the frequency, f_c is the corner frequency, n is the high-frequency fall-off and Q is the quality factor. We follow the methods described by Abercrombie (1995), Model 2, and assume $Q = 1000$ for both P and S waves (Fig. 6, Table 2).

We vary the fitting bandwidth to obtain optimal fits and also eliminate any spectra where resonances may be affecting the result. Our results are predominantly from the vertical component as this is least affected by resonance problems (Manov *et al.* 1996). We also compare spectra from clustered earthquakes to help distinguish between source, and site and path effects.

For all the clustered earthquakes we then calculate the spectral ratio between the largest earthquake in the cluster and each smaller

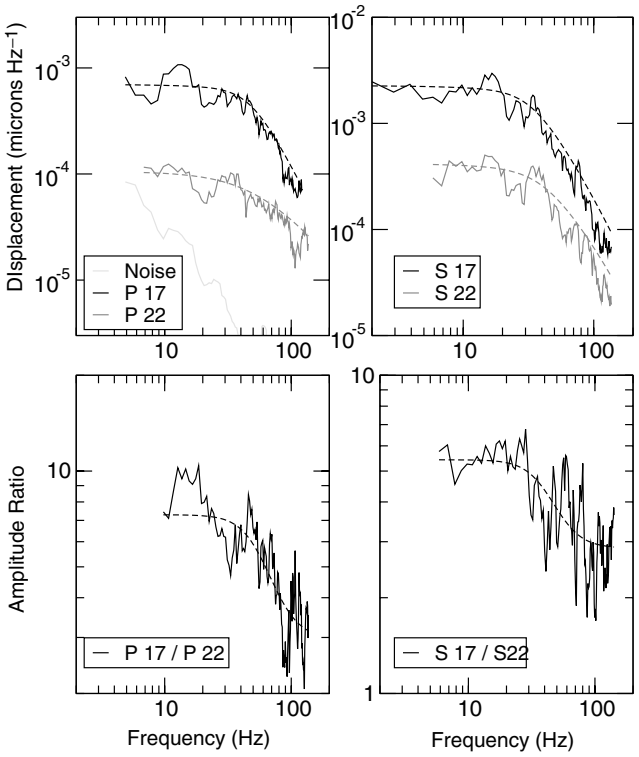

Figure 6. Source spectra of *P* and *S* waves for earthquakes 17 and 22 (Fig. 4), on the vertical component, and the spectral ratios of these two earthquakes. The corner frequencies for earthquake 17 are 48 Hz (*P*) and 34 Hz (*S*) from the displacement spectrum, assuming $Q = 1000$, and 54 Hz (*P*) and 50 Hz (*S*) from the spectral ratios. Those for earthquake 22 are 48 Hz (*P*) and 42 Hz (*S*), and 85 Hz (*P*) and 77 Hz (*S*), respectively. For these earthquakes the spectral ratio measurements imply higher stress drops.

earthquake. This is a variation on the empirical Greens' function technique (e.g. Mori & Frankel 1990) that uses the maximum amplitude data in the ratios. We refer to these ratios as EGF spectral ratios. We use both *P* and *S* waves on all three components, eliminating those affected by resonances. For cluster 2C we also calculate the spectral ratios of the smaller earthquakes to the second largest earthquake. If we assume that the ω^{-2} fall-off at high frequencies is appropriate, then we can fit these spectral ratios using

$$\frac{\Omega^1(f)}{\Omega^2(f)} = \left(\frac{\Omega_0^1}{\left[1+\left(f/f_c^1\right]^4\right)^{0.5}}\right)\left(\frac{\Omega_0^2}{\left[1+\left(f/f_c^2\right)^4\right]^{0.5}}\right)^{-1},$$

based on Boatwright (1980) where Ω^1 is the displacement amplitude, Ω_0^1 is the long-period displacement amplitude and f_c^1 the corner frequency of the large earthquake and Ω^2, Ω_0^2 and f_c^2 those of the small earthquake, respectively. We thus obtain a corner frequency for each earthquake in the ratio, and the ratio of the two earthquake seismic moments (Table 3).

3.3 Source parameters

We use the Ω_0 and f_c measurements for each individual *P* and *S* wave spectrum to calculate source parameters (Table 2) using the same method and assumptions as described by Abercrombie (1995). We use a *P* velocity (α) = 6000 m s^{-1}, *S* velocity (β) = $\alpha/\sqrt{3}$, density = 2700 kg m^{-3} and rigidity modulus (μ) = 3×10^{10} N m^{-2}. We follow Brune (1970) to calculate M_0 from Ω_0, and Madariaga (1976, 1979) to calculate source radius from the f_c, assuming circular rupture, and a rupture velocity of 0.9β. We also assume average radiation pattern corrections for both *P* and *S* waves (0.52 and 0.63 respectively). We then estimate the average slip, $S = M_0/\mu\,\pi\,r^2$, and equate this with the value obtained by Eshelby (1957) to estimate the average stress drop,

$$\Delta\sigma = \frac{7}{16}\frac{M_0}{r^3}.$$

We use the EGF spectral ratios to calculate source parameters in a similar manner (Table 3). The corner frequencies are directly converted to source dimension, using averages of the best fit values when an earthquake is included in more than one ratio. We use the individual moments calculated for the largest earthquakes in each cluster, and then use the amplitude ratios determined from fitting the spectral ratios to calculate the moments for the smaller earthquakes. The moments calculated from the spectral ratios are typically within 20 per cent of those calculated from the individual spectra, and so in all plots we use the individual values for easier comparison. The EGF ratios only provide an alternative estimate of the corner frequency and hence the stress drop.

For each earthquake we calculate an initial estimate of E_S in the same manner as Abercrombie (1995), by summing the velocity-squared spectrum after correction for attenuation ($Q = 1000$). To correct for bandwidth limitations, we then use the model source spectrum (calculated to determine Ω_0 and f_c) to estimate the energy radiated between 10^{-6} Hz and the data minimum frequency, and also between the data maximum frequency and 2000 Hz. We term the combined value the model energy for each earthquake *Add_E* (see Table 2). We check this method by calculating the energy in the model in the same frequency range as the data and comparing the data and model over the same frequency range. There is a good correspondence between the two energy values, with the data having a mean of 1.5 times (standard deviation of 0.4 times) the model. This suggests that our correction is most likely to be an underestimate. We therefore add the model energy to the initial estimates of E_S obtained from the data to obtain a bandwidth corrected estimate of the radiated seismic energy. We refer to this corrected value as E_S in the following. The model energy ranges from 3 per cent (for the largest earthquakes) to 89 per cent (for the smallest earthquakes) of the total estimate of E_S, and has a mean of 36 per cent, Table 2.

The earthquakes in Cluster 1E all have very high ratios of *P*-wave moment to *S*-wave moment (PM_0/SM_0), and recorded *P*-wave to *S*-wave amplitude, compared with the other earthquakes analysed, and with the ratios predicted using the average radiation pattern. This implies that the ray take-off angle for earthquakes in Cluster 1E is near a node in the *S*-wave radiation pattern. We attempt to use the focal mechanism determined by Hauksson (2000), Fig. 4, to correct for this, but it has the opposite effect, implying that the uncertainties in the focal mechanism and hypocentral parameters are too large for individual focal mechanism corrections to be useful here. We therefore correct the energy estimates for Cluster 1E using the ratio of the *P*- and *S*-wave moments; we multiply E_S by ([mean of other earthquakes PM_0/SM_0]/[Cluster 1E PM_0/SM_0])^2 $= 2.9^2$. This correction does not affect the relative values within the cluster, but should be remembered when comparing the cluster 1E earthquakes with the other earthquakes.

The resulting source parameters obtained from both the individual spectral measurements and the EGF ratios are compared in Fig. 7, with one another and with the results published by Abercrombie (1995). We only use earthquakes for which we

Table 2. Spectral fitting of individual spectra.

ID	Cl	M_0P	M_0S	f_cP	f_cS	nP	nS	M_0 (N m)	R (m)	$\Delta\sigma$ (MPa)	E_S (J)	*Add_E* (J)
02	2C	1.39e+14	0	5.04	0	1.80	0	1.39e+14	220.	5.72	2.08e+09	5.07e+08
03	1A	4.65e+13	0	9.48	0	1.77	0	4.65e+13	117.	12.7	0	0
04	—	0	6.41e+12	0	6.11	0	1.21	6.41e+12	119.	1.66	8.96e+07	2.40e+08
05	1B	2.97e+12	0	25.0	0	2.37	0	2.97e+12	44.3	15.0	6.10e+07	3.39e+06
07	8A	9.34e+11	1.51e+12	23.6	12.1	2.42	2.22	1.22e+12	53.5	3.49	3.81e+06	8.59e+04
08	1B	7.14e+10	2.30e+11	49.1	43.7	3.19	2.96	1.50e+11	19.6	8.72	2.32e+06	1.06e+05
09	—	6.57e+11	3.92e+11	24.3	29.5	1.51	2.31	5.24e+11	35.1	5.30	3.64e+06	7.81e+05
10	4C	3.51e+11	4.40e+11	25.0	15.2	1.91	2.21	3.95e+11	46.0	1.77	7.16e+05	4.19e+04
11	1E	8.91e+11	4.80e+11	25.5	24.8	1.74	1.35	5.29e+11	36.4	4.81	1.17e+07	1.67e+07
12	3B	2.46e+11	3.11e+11	45.8	25.2	3.49	3.13	2.78e+11	26.5	6.52	7.61e+05	2.60e+03
13	—	3.58e+11	1.45e+11	48.3	31.4	2.48	1.71	2.51e+11	23.1	8.96	1.05e+06	4.82e+05
14	—	3.30e+11	1.85e+11	30.3	49.1	1.29	2.57	2.57e+11	25.7	6.63	2.69e+06	1.30e+06
15	4C	2.80e+11	2.91e+11	22.6	16.9	2.28	2.43	2.86e+11	46.1	1.28	3.22e+05	6.18e+03
16	—	3.12e+11	0	20.7	0	1.30	0	3.12e+11	53.5	0.89	1.62e+06	5.51e+06
17	1C	1.61e+11	8.27e+10	47.7	33.6	2.05	1.87	1.22e+11	22.5	4.70	3.44e+05	1.03e+05
18	2C	2.13e+11	1.73e+11	39.1	28.8	1.56	1.49	1.93e+11	26.8	4.38	1.14e+06	1.60e+06
19	8A	1.12e+11	1.60e+11	19.6	13.3	1.75	2.00	1.36e+11	55.7	0.34	6.97e+04	5.96e+03
20	—	1.39e+10	1.88e+10	81.0	67.7	1.93	1.56	1.63e+10	12.2	3.92	7.74e+04	1.50e+05
21	1C	4.80e+10	2.60e+10	49.5	36.7	1.46	1.69	3.70e+10	21.1	1.73	5.06e+04	5.97e+04
22	1C	2.42e+10	1.52e+10	48.4	41.8	0.97	1.58	1.97e+10	20.1	1.06	2.49e+04	2.07e+04
23	1C	5.13e+10	3.23e+10	45.4	31.7	1.40	1.54	4.18e+10	23.7	1.37	5.96e+04	8.79e+04
24	2C	6.02e+09	3.96e+09	0	65.5	0	0.93	4.99e+09	11.1	1.59	1.38e+04	0
25	2C	5.96e+09	3.97e+09	0	68.1	0	1.39	4.96e+09	10.7	1.78	1.02e+04	1.45e+04
27	2C	0	6.35e+09	0	112.9	0	2.07	6.35e+09	6.4	10.4	1.85e+04	3.23e+04
28	1E	4.83e+10	0	34.4	0	1.29	0	4.83e+10	32.3	0.63	1.86e+05	4.82e+05
29	1E	2.22e+10	0	63.0	0	1.04	0	2.22e+10	17.6	1.78	2.39e+05	1.83e+06
30	1E	0	0	0	0	0	0	0	0	0	3.34e+04	0
31	1E	3.55e+10	0	40.0	0	1.49	0	3.55e+10	27.7	0.73	1.79e+05	1.81e+05
32	1A	1.51e+10	1.04e+10	65.6	30.4	2.94	2.19	1.27e+10	20.4	0.65	3.55e+03	3.78e+02
33	1A	1.96e+10	1.41e+10	55.9	35.6	2.12	2.47	1.68e+10	20.1	0.90	7.21e+03	4.09e+03

E_S is the radiated energy, including the model correction, and *Add_E* is the model addition included in E_S. Cl is the cluster and R the source radius. nP and nS are the high-frequency fall-off for P and S waves respectively. $Q = 1000$ is assumed. Note that our values of G' and σ_a can easily be calculated using the rigidity, $\mu = 3 \times 10^{10}$ N m^{-2}, and eqs (1) and (4).

Table 3. Source parameters of Cajon Pass earthquakes using empirical Green's function analysis.

Cluster	ID 1 (big)	ID 2 (small)	*AP*	*AS*	f_cP1 (Hz)	f_cS1 (Hz)	f_cP2 (Hz)	f_cS2 (Hz)	M_0 (N m)	$R1$ (m)	$\Delta\sigma$ 1 (MPa)	$R2$(m)	$\Delta\sigma$ 2 (MPa)
1A	03	32	3149	*clip*	9.31	*clip*	82.6	*clip*	1.95e+10	120*	10.8*	13.4	2.31
1A	03	33	2934	*clip*	9.13	*clip*	83.2	*clip*	2.53e+10			13.3	3.11
1B	05	08	4.76	*clip*	36.3	*clip*	60.1	*clip*	6.24e+11	30.5	45.6	18.4	36.6
1C	17	21	3.58	3.34	51.7	24.0	66.9	42.2	3.49e+10	22.3*	4.78*	16.9	3.34
1C	17	22	7.28	5.55	52.5	38.2	81.3	51.9	1.83e+10			13.8	3.26
1C	17	23	3.44	2.62	—	—	82.6	73.3	3.92e+10			11.7	11.5
1E	11	29	18.7	30.4	25.2	24.0	32.7	54.2	3.18e+10	40.4*	3.51*	23.7	0.731
1E	11	30	59.0	49.1	28.2	24.0	53.1	45.0	1.24e+10			18.5	0
1E	11	31	24.0	—	22.9	—	45.9	—	3.72e+10			24.2	1.10
1E	11	28	19.3	29.7	18.7	16.5	26.8	28.2	3.12e+10			33.6	0.567
2C	02	18	143	*clip*	8.05	*clip*	51.2	*clip*	2.43e+11	138*	23.3*	—	—
2C	02	24	6941	*clip*	12.0	*clip*	93.8	*clip*	—			11.8	1.32
2C	02	25	14380	*clip*	7.90	*clip*	85.7	*clip*	—			12.9	1.00
2C	02	27	7444	*clip*	10.0	*clip*	79.1	*clip*	—			14.0	1.01
2C	18	24	95.2	153.	50.0	40.2	70.9	77.4	6.74e+09	19.4*	11.5*	12.5	1.11
2C	18	25	90.0	144.	49.3	40.4	70.0	66.6	7.14e+09			13.4	0.906
2C	18	27	73.1	120.	55.1	45.5	76.0	93.1	8.72e+09			12.0	1.98
4C	15	10	1.10	1.38	35.6	44.2	49.9	50.6	2.33e+11	23.8	12.8	18.3	20.4
8A	07	19	8.43	8.89	54.0	27.6	77.0	36.9	1.40e+11	23.4	41.5	17.1	12.0

AP, amplitude ratio of the *P*-wave spectra; *AS*, amplitude ratio of the *S*-wave spectra. The amplitude ratios and corner frequencies are the mean of the good components (usually H1 and Z).

*The radius and stress drop of the largest earthquake is the mean of the results from all ratios for the cluster. Missing values are the result of poor fits, for example because of resonance. *clip* indicates that the wave was clipped.

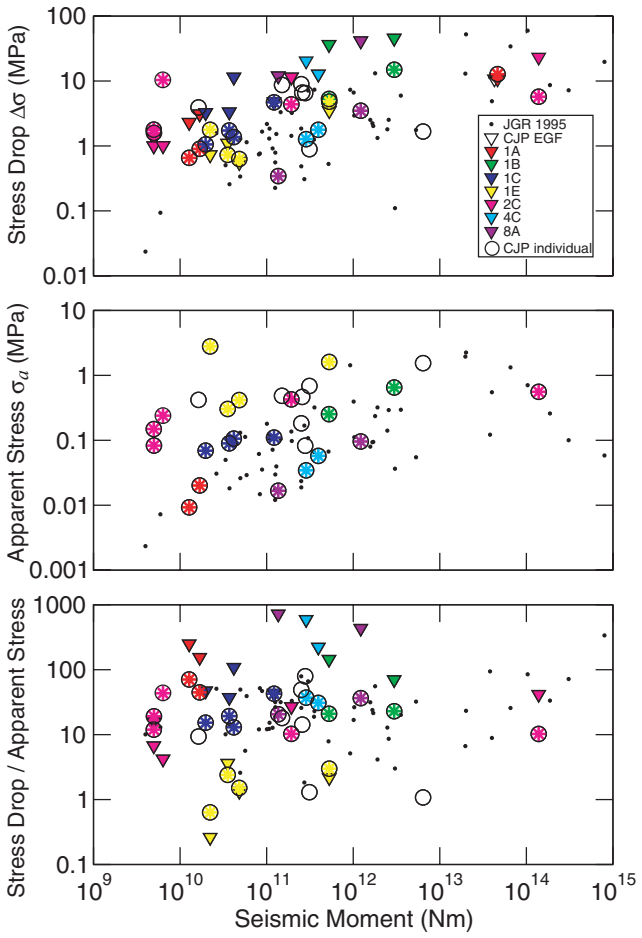

Figure 7. Comparison of source parameters determined from fitting individual spectra (circles) and spectral ratios (triangles) using the Madariaga source model. Earthquakes with the same colour are from the same collocated clusters. The black dots are the results of Abercrombie (1995), Model 2, for comparison. (a) Stress drop, (b) apparent stress and (c) the ratio of stress drop to apparent stress are plotted against moment. (The spectral ratios do not give an estimate of apparent stress so only individual values are plotted in (b).)

can estimate E_S, M_0 and $\Delta\sigma$ to avoid the selection bias of Abercrombie (1995). Colour coding enables comparison of earthquakes in specific clusters. The use of the improved technique for estimating the radiated energy has removed the selection bias for small earthquakes ($M_0 < 5 \times 10^{11}$ N m) present in the results of Abercrombie (1995). However, all the data sets still show some tendency for both σ_a and $\Delta\sigma$ to increase with increasing moment.

3.4 Comparison of EGF with individual measurements

Comparison of the EGF estimates of stress with those derived from individual spectral measurements does not show a clear trend. Ide *et al.* (2003) found that the ratio of $\Delta\sigma$ from EGF to that from individual measurements increased with decreasing moment, suggesting that the individual spectral measurements were underestimating the corner frequency for the small earthquakes recorded in the Long Valley borehole. (Ide *et al.* 2003, used *S* waves only as he was using the Brune model to estimate source parameters.) The same trend is not present in the Cajon Pass data, probably because of the lower attenuation. The Cajon Pass and Long Valley instruments were located at similar depths, but at Cajon Pass the seismometer was in a granite batholith ($Q \sim 1000$) and at Long Valley it was in a volcano ($Q \sim 250$). The earthquakes in Cluster 1E exhibit negligible difference between the two estimates of stress drop (the two methods give similar estimates of corner frequency), supporting our interpretation of the low-energy estimates for this cluster resulting from the radiation pattern and not from anomalous path attenuation. The earthquakes in Clusters 2C and 1A show opposite trends with moment. The EGF method gives significantly higher $\Delta\sigma$ for a number of earthquakes including those in Clusters 1B, 4C and 8A. These high EGF values probably result from the relatively small difference in moment between the earthquakes in these spectral ratios. All the amplitude ratios in Clusters 1B, 1C, 4C and 8A are less than 10 (see Table 3), and it is generally found that the EGF techniques work best for pairs of earthquakes differing in size by at least one magnitude unit (Mori & Frankel 1990). We therefore prefer the individual spectral results for these clusters. For consistency, we use the individual values for all the earthquakes in the rest of this study. We perform all the following analysis with both sets of parameters, however, and do not obtain significantly different results using the EGF values.

4 INTERPRETATION

4.1 Comparison of new results with previous work over a wide moment range

In Fig. 8, we combine our newly calculated source parameters (derived from individual spectral measurements) with those from a range of recent studies encompassing a wide range of earthquake sizes (Tables 4 and 5). We recalculate the results from the studies of small and moderate-sized earthquakes using the same assumptions used in our analysis, to remove systematic offsets. For example, rupture velocity is thought to be between 0.75 and 0.9β, but different authors assume different values within this range; in our analysis we assume 0.9β, as did Abercrombie (1995). We calculate the source radius and stress drop of the earthquakes studied by Ide *et al.* (2003) using both their *P*- and *S*-wave spectral measurements, the source model of Madariaga (1976, 1979) and assuming a rupture velocity of 0.9β (Table 4). Our results from Cajon Pass are in excellent agreement with these recalculated values (Fig. 8). Mori *et al.* (2003) used EGF methods to make time domain measurements of the larger aftershocks of the 1994 Northridge earthquake. These are also plotted in Fig. 8 after recalculating assuming the same rupture velocity of 0.9β (Table 4). We also include the parameters from a number of well-studied large strike-slip earthquakes (Table 5). We estimate $\Delta\sigma$ for the large earthquakes from the seismic moment and the area of slip derived from slip inversions. For each large earthquake we plot both teleseismic and regional estimates of the radiated seismic energy in Fig. 8, and where available multiple estimates of energy are plotted for individual earthquakes. For all earthquakes we assume $\mu = 3 \times 10^{10}$ N m^{-2} to calculate σ_a using eq. (1); Mori *et al.* (2003) used a depth-dependent μ which varies from 2.88×10^{10} to 5.99×10^{10} and Ide *et al.* (2003) used $\mu = 3 \times 10^{10}$ N m^{-2}.

Interpretation of Figs 8(a) and (b) is very subjective. Individual data sets show varying trends with moment, depending on whether we consider the maximum or average values in each data set. In particular, identification of any dependence of σ_a on moment depends on whether one prefers to use only the values of Ide *et al.* (2003),

Table 4. Source parameters for Northridge aftershocks and Long Valley earthquakes recalculated assuming rupture velocity of 0.9β, from Mori *et al.* (2003) and Ide *et al.* (2003) respectively.

ID	M_0 (N m)	R (m)	$\Delta\sigma$ (MPa)	E_S (J)
N3150210	7.70e+14	504	2.60	2.00e+10
N3172383	8.70e+14	540	2.49	2.30e+10
N2150608	1.00e+15	636	1.68	6.40e+10
N3140898	1.00e+15	612	1.97	8.50e+09
N2138698	1.40e+15	492	4.98	3.20e+10
N3141242	1.40e+15	696	1.85	1.20e+10
N3149105	1.40e+15	720	1.62	1.80e+10
N3145171	1.70e+15	804	1.45	2.20e+10
N3147259	1.70e+15	660	2.55	2.20e+10
N3140728	2.00e+15	636	3.47	2.30e+10
N3145168	2.20e+15	516	7.06	4.30e+10
N3143546	2.40e+15	864	1.62	2.60e+10
N3145150	2.50e+15	792	2.20	1.00e+11
N3142081	2.60e+15	792	2.31	4.60e+10
N3146628	3.20e+15	780	2.90	1.10e+11
N3195727	3.40e+15	1020	1.39	2.00e+11
N3140691	4.00e+15	708	4.98	1.20e+11
N3169078	4.60e+15	648	7.41	7.60e+10
N3142198	4.80e+15	576	10.9	1.90e+11
N3140870	5.60e+15	660	8.33	9.00e+10
N3141180	6.00e+15	744	6.25	6.90e+10
N3145627	7.50e+15	840	5.61	1.80e+11
N3140678	7.90e+15	552	20.1	1.70e+11
N3140766	1.60e+16	1596	1.74	5.20e+11
N3141597	1.70e+16	696	21.7	4.40e+11
N3142597	2.50+16	1404	3.99	2.20e+12
N3141219	3.50e+16	744	37.7	9.90e+11
N3217586	4.10e+16	2544	10.8	1.20e+12
N3159411	1.20e+17	2292	4.40	4.20e+12
I3	2.17e+11	57.7	0.50	1.99e+06
I6	3.65e+11	31.9	4.93	6.38e+06
I11	5.90e+11	36.5	5.32	9.65e+06
I12	4.28e+12	56.9	10.2	4.08e+08
I13	5.99e+10	28.6	1.12	6.75e+05
I15	2.17e+12	72.4	2.50	3.97e+07
I16	1.12e+11	32.4	1.43	1.12e+06
I17	1.02e+11	13.5	18.0	4.44e+06
I18	1.31e+13	88.7	8.22	4.33e+08
I19	6.30e+11	33.7	7.22	1.53e+07
I20	1.45e+12	51.2	4.73	2.87e+07
I21	1.43e+11	29.6	2.41	1.63e+06
I23	1.95e+11	27.6	4.07	5.32e+06
I24	5.27e+11	33.4	6.21	1.65e+07

ID is N and CUSPID for the Northridge aftershocks, and I is the ID number used by Ide *et al.* (2003) for their Long Valley earthquake study. Note that our values of G' and σ_a can easily be calculated using the rigidity, $\mu = 3 \times 10^{10}$ N m^{-2}, and eqs (1) and (4).

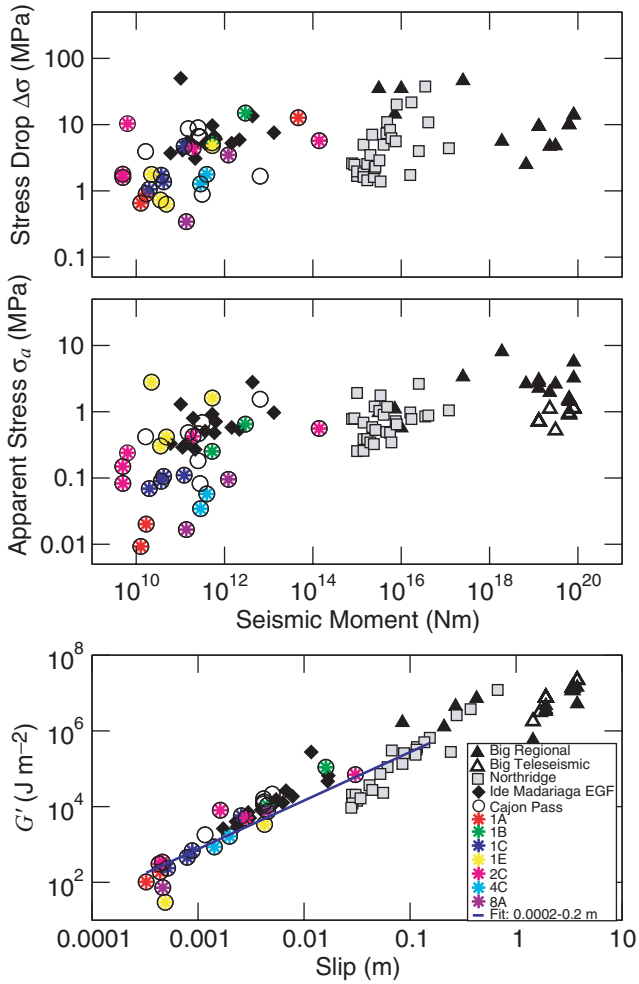

Figure 8. Source parameters determined in this study combined with those from other studies. The circles are the Cajon Pass recorded earthquakes, using the Madariaga source model and measurements on individual spectra. Earthquakes from the same cluster have the same colour. The black diamonds are the source parameters derived from spectral ratio fitting by Ide *et al.* (2003), recalculated using the Madariaga source model and both P and S measurements (Table 4). The grey squares are the larger Northridge aftershocks (Mori *et al.* 2003) calculated using empirical Green's functions and corrected to the same rupture velocity as the Cajon Pass results (Table 4). The black triangles are estimates of source parameters of larger, mostly Californian, earthquakes from a variety of studies (see Table 5). The solid symbols are regional estimates of energy and the open symbols, teleseismic. (a) Stress drop using the Madariaga source model for the Cajon Pass and Long Valley earthquakes, (b) apparent stress and (c) G', our proxy for fracture energy. The least-squares fit between 0.2 mm and 0.2 m slip (blue line) is given by eq. (5).

from a single cluster, or to include all the Cajon Pass results for small earthquakes, and on whether one prefers regional or teleseismic estimates of energy at large magnitudes. We would argue that the uncertainties in the present data do not allow us to exclude either complete self-similarity or some variation in the earthquake rupture process with moment.

4.2 Fracture energy

One way to use the source parameters to place direct constraints on the earthquake rupture process is to estimate the fracture energy G. Using our earlier definition of G (eq. 2) and Fig. 2(b) to evaluate the terms of the energy balance, we can calculate the parameter G':

$$\begin{aligned} G' &= G + (\sigma_d - \sigma_1)S \\ &= \left(\Delta\sigma - \frac{2\mu E_s}{M_0}\right)\frac{S}{2} \\ &= \frac{1}{2}(\Delta\sigma - 2\sigma_a)S. \end{aligned} \quad (4)$$

In the case where there is no under- or overshoot, $\sigma_d = \sigma_1$, and so $G' = G$.

Table 5. Large earthquake source parameters.

Earthquake	M_0 (N m)	R (km)	$\Delta\sigma$ (MPa)	E_S (J)	E_T	Reference to M_0 and R	Reference to energy
Landers 1992	8.0e+19	15	14.0	1.5e+16	3.0e+15	Wald & Heaton (1994)	Kanamori *et al.* (1993)
Landers 1992	8.0e+19	15	14.0	8.6e+15	3.0e+15	Wald & Heaton (1994)	Kanamori 2003[a]
Sierra Madre 1991	2.5e+17	5.6	46.0	2.8e+13	—	Dreger (1991)	Kanamori *et al.* (1993)
JT fshock 1992	3.1e+15	0.35	35.0	1.0e+11	—	Mori (1996)	Kanamori *et al.* (1993)
JT mshock 1992	1.9e+18	5.0	5.6	5.1e+14	—	Hough & Dreger (1995)	Kanamori *et al.* (1993)
Northridge 1994	1.3e+19	8.5	9.4	9.8e+14	3.1e+14	Wald *et al.* (1996)	Kanamori *et al.* (1993)
Northridge 1994	1.3e+19	8.5	9.4	1.3e+15	3.1e+14	Wald *et al.* (1996)	Kanamori 2003[a]
Northridge 1994	1.3e+19	8.5	9.4	1.2e+15	3.1e+14	Wald *et al.* (1996)	McGarr (2000)
Kobe 1995	2.3e+19	13	4.7	1.5e+15	8.5e+14	Wald *et al.* (1995)	Kanamori 2003[a]
Loma Prieta 1989	3.1e+19	14	4.8	2.7e+15	5.4e+14	Wald *et al.* (1996)	
Imperial Valley 1971	6.7e+18	11	2.5	5.9e+14	—	Archuleta (1984)	—
Hector Mine 1999	6.3e+19	14	10.0	3.0e+15	1.9e+15	Ji *et al.* (2002)	Venkat02[b]
Hector Mine 1999	6.3e+19	14	10.0	3.0e+15	2.0e+15	Ji *et al.* (2002)	Venkat02[b,d]
Hector Mine 1999	6.3e+19	14	10.0	3.4e+15	3.2e+15	Ji *et al.* (2002)	Boatwright *et al.* (2002)[d]
Northridge ashock 1[e]	1.0e+16	0.5	35.0	1.9e+11	—	Venkat00[c]	Ide *et al.* (2003)
Northridge ashock 2[f]	7.1e+15	0.6	14.4	2.6e+11	—	Venkat00[c]	Ide *et al.* (2003)

E_S is the regional estimate of the radiated energy and E_T is the teleseismic estimate. All teleseismic energy values are from Choy and Boatwright (NEIC monthly PDE listings) unless noted otherwise. R is equivalent source radius calculated from the slip area.
Note that our values of G' and σ_a can easily be calculated using the rigidity, $\mu = 3 \times 10^{10}$ N m^{-2}, and eqs (1) and (4).
[a]Personal communication. [b]Venkataraman *et al.* (2002). [c]Venkataraman *et al.* (2000). [d]Regional and teleseismic. [e]1997 April 26. [f]1997 April 27.

We can calculate G' from our estimates of the source parameters, and the resulting values are plotted in Fig. 8(c). We observe a clear increase in G' with increasing slip, up to slips of about 0.5 m. At larger slip it is unclear whether G' continues to increase or reaches a constant maximum value. Further work is required to clarify which estimates, teleseismic or regional, of large earthquake radiated energy are more correct (e.g. Boatwright *et al.* 2002; Venkataraman *et al.* 2002).

Since the plot is logarithmic, the 14 earthquakes with negative G' are not plotted. They are evenly distributed across the whole moment range, with absolute values similar to the positive values for earthquakes with similar moment. The individual data sets show slightly offset trends to the combination. Although fracture energy is often considered a material constant, and thus scale invariant, this is not in fact the case (e.g. Ohnaka 2003). Our estimates of G', and also of its tendency to scale with earthquake size, are consistent with seismic estimates of fracture energy made by very different methods for large earthquakes (Husseini *et al.* 1975; Beroza & Spudich 1988; Rudnicki & Wu 1995; Rice 2000; Guatteri *et al.* 2001; Ide 2002; Rice *et al.* 2004), and also with laboratory data; see the Discussion section. Such considerations suggest that our inferred values of G, as G', are reasonable.

We fit the G' values in the slip range 0.2 mm and 0.2 m and obtain a relationship between G' and the slip (S) of the form

$$\log_{10}(G') = 1.28 \log_{10}(S) + 6.72, \quad (5)$$

or $G' = 5.25 \times 10^6 S^{1.28}$,
where G' is in J m^{-2} and S is in m. Differentiating eq. (2) gives

$$\frac{dG'(S)}{dS} = -S\frac{d\sigma(S)}{dS}.$$

We can then combine this relationship with the result in eq. (5) to derive a slip-weakening function

$$\sigma_F(S) = C - 24S^{0.28}, \quad (6)$$

where stress is in MPa and slip in m. The exact power laws should not be taken too literally, but only to describe how highly scattered data scales in an average sense with slip. The constant C is not determined by our present analysis. It is unlikely that our fit could be extended all the way to slip $S = 0$, since rate- and state-weakening effects active over the first few tens of micrometres are likely to be important there. Nevertheless, approximately extending the power law fit to $S = 0$ allows the identification that $C = \sigma_p$, the peak strength at onset of failure. Such a function, as defined by eq. (6), is plotted in Figs 2(b) and 3(d). More generally it could be argued that C should be the strength remaining after some multimicrometre-range slip which suffices to slide the long-lived (and hence strong) population of microscopic frictional contact asperities out of existence, and replace them with new weaker ones. In such an interpretation C would be a lower bound to σ_p, i.e. $\sigma_p > C$. We provide some quantification of the possible magnitude of $\sigma_p - C$ in Section 5.9. We assume, arbitrarily, that $C = \sigma_p = 100$ MPa for purposes of plotting this function in Fig. 9. Although $\sigma_F(s)$ continues to decrease with increasing slip, at each scale in Fig. 9 it appears to have flattened off, thus leading to an apparent increase in D_c. In the above we have assumed $G = G'$, i.e. $\sigma_1 = \sigma_d$. If $\sigma_1 > \sigma_d$ (partial stress drop) then this value of G can be considered a minimum. Also, we have no data for $S < 0.2$ mm or so. Hence we can say nothing about the slip-weakening function at these small slips.

This model of non-linear slip weakening requires that both $\Delta\sigma$ and σ_a increase with increasing M_0. They do not need to do so at the same rate, however, and the dependence of G' on slip can be modelled with $\Delta\sigma$ increasing at less than half the rate of the σ_a, consistent with the plots in Fig. 8.

The principal result of this analysis is that there need be no relationship between the friction parameters of the fault and the amount of slip in the earthquake. If slip weakening occurs in a similar manner to that shown in Fig. 9, then the concept of D_c becomes rather meaningless. Given the uncertainties in the slip-weakening function, and also in the methods used to retrieve dynamic source parameters from strong motion seismograms (Guatteri & Spudich

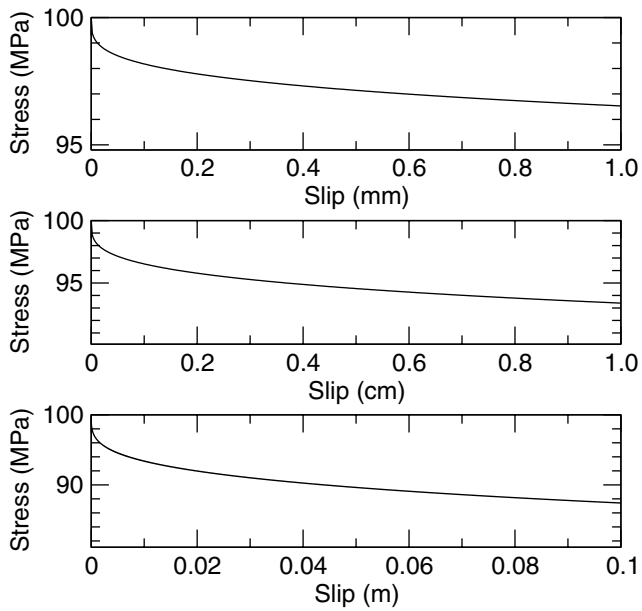

Figure 9. Dynamic stress level and frictional resistance derived from fitting G' and slip (Fig. 8c) plotted for three different slip ranges. Note that in each plot the function appears to level off at large slips. The stress level is plotted relative to an arbitrary peak stress of 100 MPa.

2000), it might be better for such studies to aim to estimate G rather than D_c.

5 DISCUSSION

The results of this study show that there are still large uncertainties in our understanding of earthquake rupture. The results do enable us to place some constraints on the process, however, and point to areas where further work will enable greater clarification. Within present uncertainties, earthquakes could be purely self-similar, or the rupture could depend on the size of the earthquake in a number of different ways. For example, there could be a continuum with friction gradually decreasing with increasing slip, or there could be a rapid drop in friction at large slip, or the breakdown slip, D_c could increase with increasing earthquake size.

To place further constraints on earthquake rupture dynamics, the following questions need to be addressed.

5.1 Varying resolution across earthquake range

One problem with comparing source parameter measurements over such a wide range of scales is the different resolution of the various studies. Source parameters such as seismic energy are at best known within a factor of two or so, and therefore the total energy radiated by, for example, an $M3$ earthquake, would be lost in the uncertainties in the measurement of the energy radiated by an $M6$ earthquake. Since the estimates of G' made here are of similar order to the estimates of E_S it is possible that we are simply plotting the errors in the measurements of E_S, which decrease in absolute (although not relative) terms across the magnitude range. The fact that there are significantly more positive values of G' than negative ones suggests that we are not simply plotting uncertainties, but we must be aware of the relative scaling of uncertainties in our interpretation. For example, if all the earthquakes had a fracture energy of say 10^3 J m^{-2}, then it would be impossible to resolve it for all but the smallest earthquakes.

5.2 E_S for large earthquakes

Fig. 8 shows some of the discrepancies between teleseismic and regional estimates of E_S for large earthquakes. Until this issue is resolved we will not have a good understanding of the earthquake energy budget. Initially it seemed most likely that the teleseismic estimates were incorrect, either because of focal mechanism corrections (Pérez-Campos & Beroza 2001) or the large attenuation corrections needed (e.g. Singh & Ordaz 1994). Boatwright *et al.* (2002) and Venkataraman *et al.* (2002) considered the effects of frequency-dependent regional attenuation for the Hector Mine earthquake and found that the regional energy estimates of some earthquakes may be too high. Perez-Campos *et al.* (2003) also found that initial regional estimates for Mexican subduction earthquakes were overestimates.

5.3 Brune versus Madariaga source model

Two simple rupture models are in common usage for determining earthquake source parameters from the spectral measurements of Ω_0 and f_c. Brune (1970) used a simple but somewhat *ad hoc* hypothesis to associate a rupture diameter with a corner frequency, and then used a static crack model to infer the stress drop corresponding to the moment and that diameter. Madariaga (1976, 1979), in contrast, used an actual dynamic fracture simulation to associate the diameter with the radiated signal and corner frequency. The Madariaga model was nevertheless simplified in that rupture nucleated at the centre of a circular region and propagation stopped simultaneously everywhere around the rupture front. The principal difference between these two models in their usage is that the rupture radius derived from the S-wave spectra using the Brune model is 1.76 $\times$ that obtained using the Madariaga model. Therefore, the stress drops obtained using the Madariaga model are 5.5 times those from the Brune model. The Madariaga model also includes P waves and predicts a ratio of P to S corner frequencies of 1.5 which is close to that observed here (mean of 1.45), and also in many previous studies, for example Abercrombie (1995) and Ide *et al.* (2003). Later workers extended the Brune model to P waves by assuming a corner frequency ratio of 1.5. The model of Sato & Hirasawa (1973) is also in use and predicts radii and stress drops approximately mid-way between the Brune and Madariaga models.

In this study we prefer the Madariaga model. It is a dynamic model, and the predicted corner frequency ratio is in good agreement with that which we observe. Also, visual observation of breakthroughs of mine walls, or targeted excavations, can sometimes be used to assess the dimensions of shear rupture in the mining environment. Gibowicz & Kijko (1994) (see their section 11.5, pp. 284–291) comment that the source radii calculated by the Brune model tend to be unrealistically large, whereas the Madariaga model provides reasonable results when compared with the independent observations. Ide *et al.* (2003) used the Brune model to calculate source parameters and so obtained lower values than those plotted in Fig. 8. The difference is less than a factor of 5 because we use both P and S spectra for the Madariaga model whereas Ide *et al.* (2003). used only S waves for the Brune model. The ratio of P to S corner frequencies in the Long Valley data is 1.35, excluding two very high values (4 and 9). Ide *et al.* (2003) used only S waves and the Brune model to obtain $\Delta\sigma/\sigma_a$ ratios for the small earthquakes of about 3, compared with the factor of 10 that we calculate here. The average $\Delta\sigma$ that they obtain (2 MPa) is lower than that of the moderate sized earthquakes, so there is still a discrepancy in the results from simple self-similarity. If we recalculate the parameters for the earthquakes considered here using the Brune model, then we obtain stress drops

with a mean of 1 MPa, a factor of five lower than those presented here. The data for large earthquakes in Fig. 8 suggest that a ratio of $\Delta\sigma/\sigma_a$ of about 10 is reasonable if the teleseismic energy measurements are correct. Pérez-Campos *et al.* (2001) found an average σ_a of 0.7 MPa for large strike-slip earthquakes. If the ratio of $\Delta\sigma/\sigma_a$ is 10, this would imply an average stress drop for large strike-slip earthquakes of 7 MPa, and if the ratio is 3, then it would imply an average stress drop of 2.1 MPa. Both of these values are reasonable. When we recalculate G' using the Brune model stress drops for the small earthquakes we obtain a larger number of negative values (six compared with four for the Cajon Pass recordings, one for the Ide *et al.* (2003) results and seven compared to one for the results from Prejean & Ellsworth (2001)). We can still use these values of G' to investigate slip weakening and obtain a very similar model to eq. (5) ($\log_{10}(G') = 1.59.\ \log_{10}(S) + 6.89$).

The different values of $\Delta\sigma/\sigma_a$ imply, from eq. (4), that $G' = 4\ E_S/A$ when we use the Madariaga model, and $G' = 0.5E_S/A$ when we use the Brune model.

Both the Brune and Madariaga models are in current use for interpreting seismic data with no consensus as to which gives the most accurate results. It will take improved recording with multiple stations and the use of time-domain modelling to resolve the ambiguity definitively. Nevertheless, it must be remembered that the Madariaga model, which incorporates some aspects of dynamic rupture physics, was developed out of an attempt to evaluate the more *ad hoc* procedures used by Brune.

5.4 Focal mechanism and directivity

Studies of large earthquakes show that measurements of energy vary significantly with radiation pattern and directivity. The Madariaga model also predicts that the corner frequency varies with source orientation. The lack of reliable focal mechanisms and multiple station recordings for small earthquakes thus adds to the uncertainty in the results. Developing techniques to obtain more precise focal mechanisms of clustered earthquakes (e.g. Hardebeck & Shearer 2002), combined with plans to install multiple instruments in deep holes (e.g. SAFOD) in well-instrumented areas, should decrease these uncertainties in future.

5.5 Rupture velocity

Throughout this work, and that of previous studies, we assume the rupture velocity to be constant, independent of earthquake size. Studies of large earthquakes find that the average rupture velocity is relatively stable, varying from $\sim$0.7 to 0.9β. Studies of smaller earthquakes ($M3$ to $M4$) have obtained similar results (Frankel & Kanamori 1983; Mori 1996). Three preliminary studies of smaller earthquakes have found that the rupture velocity appears to be constant at around $0.7–0.9\beta$ to very small magnitudes. Yamada *et al.* (2002) located subevents, and performed slip inversions of earthquakes in the South African deep gold mines ($M0–1.5$), Imanishi *et al.* (2004) used stopping phases to investigate borehole-recorded earthquakes ($M1.2–2.6$) in West Nagano, and Tomic *et al.* (2003) used pulse widths and directivity to study reservoir-induced earthquakes in Brazil ($M1.8–2.2$) . If these studies are not representative, then it is possible that rupture velocity is smaller for the smaller earthquakes. At first glance it might appear that a decreased rupture velocity could explain the trends seen in Figs 1(b), 7(b) and 8(b), by predicting lower radiated energy for the smaller earthquakes. If the rupture velocity of smaller earthquakes was sufficiently smaller to match the trend in apparent stress, then it would mean that we are significantly underestimating the stress drops. If the slip expanded at a smaller rupture velocity, then it would reach a smaller source dimension in the duration of the recorded pulse, and the stress drop over the slip area would be much higher (Kanamori & Heaton 2000). A significant decrease in rupture velocity is one method of reconciling waveform observations with the results of Nadeau & Johnson (1998) who used the slip rate and timing of recurring earthquakes to estimate kilobar stress drops for microearthquakes at Parkfield. It introduces significant other problems, however, including how the faults can sustain such stresses, and there are other interpretations of their results (e.g. Sammis & Rice 2001). The assumption that rupture velocity is magnitude independent thus seems the most appropriate until convincing evidence suggests otherwise.

5.6 Laboratory experiments and characteristic slips for weakening

Our results show that dynamic failure is already under way at slips S of the order of 0.5 mm or less (see Fig. 8c). We also show that a single slip-weakening function governing small and large earthquakes is consistent with current observations. If a function similar to that in eq. (6) and Fig. 9 is correct, then it suggests that earthquake nucleation occurs at very small slips. These slips could plausibly be of the 0.01 to 0.1 mm range seen in laboratory friction experiments (Dieterich 1979, 1981; Ruina 1983; Tullis & Weeks 1986; Marone 1998), and thought to correspond to renewal of the population of contact asperities sliding long-lived, hence strong, asperities out of existence and replacing them with shorter- Dieterich & Kilgore 1994). The S of 0.5 mm is also large enough to allow the initial slip weakening of intact rock (Rice 1980; Wong 1982, 1986). Thus it is plausible that one or perhaps a combination of these processes provides the initial strength loss that promotes the instability. Our results imply that strength loss may continue with the ongoing unstable dynamic sliding during the earthquake.

To be consistent with the gradual weakening that we have inferred, eq. (6) and Fig. 9, it seems possible that there may be a cascading sequence of weakening processes which take place over possibly overlapping slip scales. That may be true even in the nucleation stage if well-slid parts of a fault, analogous to a laboratory friction surfaces, go unstable in the 0.01 to 0.1 mm range, but other regions, e.g. at stepovers, respond more like intact rock and require slips of the order of 0.5 mm. With regard to apparently non-thermal weakening processes at larger slips, recent laboratory experiments by Chambon *et al.* (2002) and Goldsby & Tullis (2002) explored large slips up to several metres and faster slip speeds than typical of most laboratory friction studies (e.g. 0.1 mm s^{-1} in the former study and 3 mm s^{-1} in the latter, although both are still small compared with the m s^{-1} range of earthquakes). They both found that friction continues to decrease beyond the initial drop seen in earlier friction experiments. The rapid fall-off of a power-law dependence of friction on slip like in Fig. 9 is, very roughly, consistent with their results. What is superposed on those processes at realistic seismic slip rates, however, is that heat is generated faster than can be conducted away and this leads to two sources of weakening. First, pore fluids in the fault zone will tend to expand much more than the mineral host and, if drainage is not possible on the seismic timescale, pore pressure is generated which reduces the effective stress (Sibson 1973; Lachenbruch 1980; Mase & Smith 1987). Here a characteristic slip length for weakening in conditions for which there is negligible drainage from the layer of shearing fault gouge to its surroundings is of the order of six to eight times the thickness of

that layer (twice the e-folding length in the Lachenbruch analysis of that case), which amounts to perhaps 10 to 100 mm. However, the characteristic weakening length may be almost arbitrarily larger if there is drainage. It is likely that damage off the main fault plane associated with sliding (Poliakov *et al.* 2002; Rice *et al.* 2004) will increase permeability and promote drainage, such that the effective normal stress cannot be reduced to negligible values. Then temperature will continue to rise and melting begins. However, due to the short timescale this will be non-equilibrium melting of the multimineralic assemblage within the fault gouge (Sibson 1975; Spray 1993, 1995). The lowest melting point components will melt first and partially weaken the gouge but only with the ongoing sliding that is needed to generate continued temperature rise will more refractory components melt, finally liquefying the gouge. Thus this may likewise be a process which takes place over a broad range of slips. We propose the possibility that these various weakening processes, acting in possibly overlapping regimes of slip, could be responsible for the continued weakening with ongoing slip that we infer.

5.7 Undershoot or overshoot?

In our modelling thus far, as in many previous studies, we assumed that the final static stress is equal to the final frictional stress. The observations cannot rule out more complex models involving partial stress drop (undershoot) or overshoot, in which the final stress is higher or lower, respectively, than the final frictional stress. Mori *et al.* (2003) calculated dynamic stress drop from the initial slope of the velocity source–time functions for the Northridge aftershocks. They found that the dynamic and static stress drops are of similar magnitude, arguing for only small overshoot or undershoot in the middle of the magnitude range we consider here. Beeler *et al.* (2003) used an energy balance method similar to that used here and found that the results published by Abercrombie (1995) indicated that the Cajon Pass earthquakes had positive overshoots and lower efficiencies than laboratory sliding events. If overshoot decreases from large values for small earthquakes to small or negligible values for large earthquakes, then it could explain the possible variation in the ratio of apparent stress to stress drop from large to small earthquakes. There is no evidence for this occurring, but $\sigma_d - \sigma_1$ is not an easy parameter to measure. Eq. (4) shows that if $\sigma_d - \sigma_1$ scales with magnitude in the same way that stress drop $\Delta\sigma$ does, then the fracture energy (G) will have the same dependence on slip as G', but will be larger than G' in the case of undershoot and smaller in the case of overshoot.

In the case of overshoot as it occurs in the simple crack models discussed in Section 2, with abrupt arrest of a fast-moving rupture front, the Madariaga (1976) analysis suggests that $\sigma_d - \sigma_1$ does scale in this manner and is approximately $\sigma_d - \sigma_1 = 0.15\Delta\sigma$. Thus if we write eq. (4) as $G' = G + (\sigma_d - \sigma_1)\ S = (0.50\Delta\sigma - \sigma_a)\ S$, then $G = (0.35\Delta\sigma - \sigma_a)\ S$. Since the mean value of $\sigma_a/\Delta\sigma$ is about 0.1, that corresponds to $G' = 0.40\Delta\sigma\ S$, and to $G = 0.25\Delta\sigma\ S$, i.e. to the same power-law $\sigma_F(S)$ expression as in eq. (6) but with the 24 replaced by 15.

More generally, we could assume that $|\sigma_d - \sigma_1|$ scales with $\Delta\sigma$, for a given set of earthquakes of a given rupture mode (crack-like, self-healing, etc.) and define $\lambda = (\sigma_d - \sigma_1)/\Delta\sigma$. When there is there is undershoot $\lambda < 0$ and when there is overshoot $\lambda > 0$ (but with expected upper limit of $0.15 \geq \lambda$ based on Madariaga 1976). Then, continuing to use $\sigma_a/\Delta\sigma = 0.1$ our eqs (4) and (5) become

$$G' = G + \lambda\Delta\sigma S = 0.40\Delta\sigma S = 5.3S^{1.28},$$

where now G and G' are in MJ m^{-2}, $\Delta\sigma$ is in MPa and S is in m. We thus solve for

$$\Delta\sigma = 13S^{0.28} \tag{7}$$

in the scaling range, a result that is independent of λ, i.e. of whether or not $\sigma_d = \sigma_1$; it expresses a systematic statistical scaling of stress drop for smaller earthquakes. Also,

$$G = (1 - 2.5\lambda)5.3S^{1.28}, \tag{8}$$

and by an argument similar to that leading to eq. (6),

$$\sigma_F(S) = C - (1 - 2.5\lambda)24S^{0.28}. \tag{9}$$

When $\lambda = 0.15$, that is consistent with the result stated at the end of the previous paragraph.

5.8 Fracture energy comparisons

We can address and, we argue, dismiss the possibility that G is actually negligible compared with G'. In this case the first equality of eq. (4) would effectively reduce to $G' = (\sigma_d - \sigma_1)S$. However, it is still the case that the second equality there holds, namely, $G' = (0.5\Delta\sigma - \sigma_a S$, which becomes $G' = 0.4\Delta\sigma S$ for our mean value $\sigma_a/\Delta\sigma = 0.1$. Thus, if $G \ll G'$, we must have $\sigma_d - \sigma_1 = 0.40\Delta\sigma$ (i.e. $\lambda = 0.4$), which is much higher than the theoretical estimates of $\sigma_d - \sigma_1$ just cited, giving the plausible upper bound $0.15 \geq \lambda$. Further, those estimates were made for abrupt arrest of a fast-moving rupture front at a barrier. Instead, larger earthquakes are expected to arrest gradually at their downdip edge as the rupture penetrates into hotter, inherently stable, parts of the fault zone where the fault walls experience a negative local stress drop (Tse & Rice 1986; Lapusta & Rice 2003). The dynamic overshoot, if any, in such cases should be less than for abrupt arrest. Thus we think we can regard overshoots as large as $\sigma_d - \sigma_1 = 0.40\Delta\sigma$ as being untenable, and hence can argue that G cannot be negligible (or even moderately small) compared with G'. If we assume that the Madariaga overshoot $\sigma_d - \sigma_1 = 0.15\Delta\sigma$ is indeed an upper bound, then G would have to be greater than 60–65 per cent of G'. What we cannot do, especially for large earthquakes, is to rule out dynamic undershoot, or partial stress drop, which makes $\sigma_d - \sigma_1 < 0$ and hence makes $G > G'$. The expression for G in eq. (8) quantifies how different degrees of undershoot ($\lambda < 0$) increase G relative to G', and of overshoot ($\lambda > 0$) decrease it.

Nevertheless, if there is such an excess of G relative to G', it is likely to be small. Our values of G' are consistent with estimates of fracture energy needed to produce geological observations of deformation in fault zones (Shipton & Evans 2003). Also, our values of G' are in the range of independently estimated values of G for large earthquakes. At the end of what is shown as a scaling range in Fig. 8(c), around slip $S = 0.5$ m, our results as summarized by equation (5) show $G' = 4$ MJ m^{-2}. Values for larger earthquakes scatter about that value and range from 0.6 to 20 MJ m^{-2} (Fig. 8). As comparisons with our G' results, Beroza & Spudich (1988) estimated from a seismic slip inversion that $G = 2$ MJ m^{-2} for the 1984 Morgan Hill earthquake, and Guatteri *et al.* (2001) similarly found 1.5 MJ m^{-2} for the 1995 Kobe earthquake, consistent with Ide (2002). Olsen *et al.* (1997) and Peyrat *et al.* (2001) estimated $G = 5$ MJ m^{-2} for the 1992 Landers earthquake. Also, for the seven earthquakes for which Heaton (1990) reported a slip inversion, with slips S ranging from 0.32 to 2.8 m, Rice *et al.* (2004) find $G = 0.1$–9 MJ m^{-2}, with an average for the set of 2–4 MJ m^{-2}. Their method was to fit a theoretical model of a self-healing rupture in a slip-weakening solid

to Heaton's inferred values of slip, rupture speed and pulse duration. Because they regarded it as unknown whether the slip-weakening zone was confined to the immediate vicinity of the fracture front or, rather, extended substantially over the slipping part of the rupture surface, each of their estimates gave bounds $G_{\min}$ and $G_{\max}(= 2\ G_{\min})$ to G, where $G_{\min}$ applies for the confined slip-weakening zone and $G_{\max}$ for the broadly extended one. (For the 1984 Morgan Hill earthquake, with $S = 0.44$ m, Rice *et al.* obtained $G = 1.3$–2.6 MJ m^{-2}, comparable to the 2 MJ m^{-2} by Beroza & Spudich. For the 1979 Imperial Valley earthquake with $S = 0.56$ m, Rice *et al.* obtained $G = 0.88$–1.9 MJ m^{-2}, whereas Favreau & Archuleta reported 0.81 MJ m^{-2}.) In addition to finding G values in the range of our G' here, there is also a tendency in the Rice *et al.* (2004) results for earthquakes with larger slips to have larger G, consistent with the scaling that we have found in G' here. For example, for the three earthquakes in the Heaton (1990) set with the largest slips Rice *et al.* (2004) find: 1983 Borah Peak, $S = 0.96$ m, $G = 1.9$–3.8 MJ m^{-2}; 1971 San Fernando, $S = 1.4$ m, $G = 4.6$–9.2 MJ m^{-2}; 1985 Michoacan, $S = 2.8$ m, $G = 4.4$–8.8 MJ m^{-2}. In comparison, for the three with smallest slip, the results are: 1979 Coyote Lake, $S = 0.32$ m, $G = 0.38$–0.76 MJ m^{-2}; 1986 North Palm Springs, $S = 0.34$ m, $G = 0.1$–0.2 MJ m^{-2} (these may be low because of a mis-estimate of rupture speed; the results of Rice 2000); 1984 Morgan Hill, $S =$ 0.44 m, $G = 1.3$–2.6 MJ m^{-2}.

Thus while we cannot rule out on *a priori* grounds that G is greater than G' (undershoot), or perhaps as much as 40 per cent less than G' (overshoot), the evidence suggests that G' is comparable to independent seismic estimates of G for large earthquakes, and, within the uncertainties of those estimates (not yet well quantified), we may take G' as a plausible proxy for G.

For small slips, we can compare our results for G' with laboratory estimates of G, which have been extensively surveyed by Wong (1986) and Li (1987). Those surveys cover a wide range of normal and confining stresses, sometimes too large to be of interest for typical crustal earthquakes, and often too small. Some experiments are on initially intact rock (typically at large confining stress to produce a localized shear failure for which the$G$ is determined) whereas others are on interfaces such as natural joints or sawcuts, sometimes filled with gouge. The range of slips in the laboratory experiments has been too small to quantify effects of slip on G as we suggest here. Wong (1986) shows results on the scaling of G with normal stress. Those cannot be summarized in a simple manner over a broad range, except for initially intact rock (Fichtelbirge granite) at normal stresses >200 MPa. We are concerned with normal stress in the 50 to 300 MPa range, which would correspond to the effective overburden pressures for crustal earthquake like those we analyse, assuming hydrostatic fluid pressure. For the initially intact granite experiments in that range, Wong (1986) reports $G = 4 \times 10^3$ to 2×10^4 J m^{-2}; the range is 4–8×10^3 J m^{-2} for normal stresses less than 150 MPa. Since the slips to achieve weakening in those Fichtelbirge granite experiments are typically of order 0.5 to 1.0 mm, and total slip in the experiments is only modestly greater than that, if at all, we should probably compare with our G' in Fig. 8c for earthquakes in the roughly 1 to 3 mm range of slips. In that range we find$G' = 10^3$ to 10^4 J m^{-2}. That is comparable to, but generally smaller than, the range of laboratory G just cited, although it must be remembered that the laboratory data are for initially intact rock.

The G for sliding on pre-existing friction interfaces or faults should certainly be lower than for the initially intact case but how much lower is hard to quantify. Wong (1986) suggested that for rough interfaces at high normal stress, such as greater than 200 MPa, the response should approach that for the intact case. That is consistent with data on Westerly granite from which Wong inferred upper and lower bounds to G of 8×10^3 to 3×10^4 J m^{-2} around 200 MPa (rather imprecise bounds since the stress versus slip relation was not well recorded during the stick slip events). Unfortunately, the range of normal stress from 40–200 MPa, probably corresponding to most of the earthquakes which we consider, is not well characterized. However, at normal stresses below 40 MPa and for sliding on highly polished Westerly granite surfaces, Wong (1986) inferred bounds which amount to 30 to 300 J m^{-2} around 40 MPa normal stress. He suggested that the relevant slip-weakening distance in those experiments was of the order of 0.025 mm, which is well below the range of slips for our data in Fig. 8(c). It is curious, but possibly just coincidental, that the range of 30 to 300 J m^{-2} for G is compatible with the range of G' that we infer for the smallest slips in our data set in Fig. 8(c).

The laboratory data are not as complete as we would wish. However, no experiments to date compel the viewpoint that the G measured at a given slip range in the laboratory, for a realistic range of normal stresses, is significantly different (say, by an order of magnitude) from the G'that we infer seismically for that slip range.

5.9 Strength excess

Our estimates of slip weakening are relative to a peak stress, but this is unknown. We can, however, use our results to put some constraints on its size. One method is to assume that σ_d, or $\sigma_F(S)$, for the large earthquakes ($S \geq 0.5$ m, towards the end of the scaling range identified in Fig. 8c) is non-negative, $\sigma_F(0.5\text{ m}) \geq 0$. Then eq. (6) with $C = \sigma_p$ shows that $\sigma_p \geq 20$ MPa. That argument has assumed that $\sigma_d = \sigma_1$ and, strictly, the bound should be thought of as applying to C so that we have $\sigma_p \geq C \geq 20$ MPa. Using the generalization in eq. (9) that inequality becomes $\sigma_p \geq C \geq 20\ (1\text{–}2.5\lambda)$ MPa when there is overshoot or undershoot. However, when there is overshoot, the condition $\sigma_F(0.5\text{ m}) \geq 0$ does not assure that $\sigma_1 \geq 0$. If it is thought reasonable to assume that $\sigma_1 \geq 0$ for large earthquake, in the sense that, for example, left-lateral aftershocks are uncommon along right lateral ruptures, then the inequality when $\lambda > 0$ strengthens slightly, to $\sigma_p \geq C \geq 20\ (1\text{–}2.0\ \lambda)$ MPa. That gives $\sigma_p \geq C \geq$ 14 MPa when $\lambda = 0.15$.

Another perspective on how relatively large is the peak strength is obtained by using eqs (7) and (9), to eliminate S, and obtain $\sigma_p - \sigma_d \geq C - \sigma_d = 1.8\ (1\text{–}2.5\lambda)\ \Delta\sigma$.

The inequalities of the last two paragraphs, together with the average stress drop $\Delta\sigma$ of order 7 MPa, imply that most of the rupture area of large earthquakes is stressed well below the critical level prior to the rupture, by at least an amount of order $\Delta\sigma$. It is only the dynamic stress increase from the propagating rupture front that pushes much of the fault to failure.

Andrews (1976, 1985) defined a ratio commonly called S in seismology but which we will call S_{seis} here, defined by $S_{\text{seis}} = (\sigma_p - \sigma_0)/(\sigma_0 - \sigma_d)$. He showed that the mode II rupture speed in 2-D numerical simulations, employing a linear slip-weakening law like that shown in Figs 3(a) and (b), remained sub-Rayleigh at sufficiently large S_{seis}, but underwent a transition to a supershear propagation speed at sufficiently small S_{seis}. The critical value was $S_{\text{seis}} = 1.7$–1.8 in his simulations, although ruptures simulated at only slightly smaller S_{seis} can propagate over a distance which is many times the critical crack size (based on the slip-weakening law and prestress) before undergoing the transition. At present the transition condition is incompletely documented in 3-D and is not at all documented for slip-weakening laws of the type in our eqs (6) or(9). Nevertheless, if we assume no undershoot or overshoot ($\lambda > 0$), and

that $\sigma_p = C$, then our $S_{seis} = 0.8$, based on $\sigma_p - \sigma_d = 1.8\Delta\sigma$ and $\sigma_d = \sigma_1$. That is sufficiently low that if the Andrews critical range 1.7–1.8 applies, then supershear rupture speeds should be observed routinely in nature. There is growing evidence for some large earthquakes reaching supershear rupture for part of their duration (e.g. Bouchon & Vallée 2003), but supershear rupture is not a common phenomenon of all earthquakes.

It is likely, however, that $\sigma_p > C$ due to weakening during the initial multimicrometre-scale slip, in which case $S_{seis} = 0.8 + (\sigma_p - C)/\Delta\sigma$. We may observe that a $\sigma_p - C > \Delta\sigma$ would then suffice to make $S_{seis} > 1.8$ and force sub-Rayleigh rupture. That threshold magnitude $\sigma_p - C = \Delta\sigma$ corresponds to a very small reduction of friction coefficient. For example, if the effective normal stress were 180 MPa (overburden at 10 km depth minus hydrostatic pore pressure) and $\Delta\sigma = 9$ MPa, then the $\sigma_p - C$ of 9 MPa would correspond to a reduction of the friction coefficient by only 0.05 during the early slip. Changes of the friction coefficient of that order and larger are routinely anticipated in rate and state characterizations of earthquake nucleation and propagation (Dieterich 1986; Tse & Rice 1986; Cocco & Bizzarri 2002; Lapusta & Rice 2003). They are the effect of replacing an ancient set of contact asperities, existing through all or much of the interseismic period, with new short-lived ones. In the conventional rate and state notation, that change in friction coefficient would be approximately $b\ \ln(R)$ where R is the ratio of the average asperity contact lifetime before slip to that after enough slip to effectively renew the population (e.g. Cocco & Bizzarri 2002). Experiments (Tullis & Weeks 1986; Blanpied *et al.* 1995; Marone 1998) show $b > 0.01$ but even using $b = 0.01$, a reduction of the friction coefficient by 0.05 would already be achieved by lifetime ratios $R > e^5 = 150$. From another perspective, Wong (1986) surveys friction experiments on relatively smooth laboratory faults of Westerly granite with normal stresses in the range 5–40 MPa. Those routinely showed stick-slip events involving slips that are typically less than about 0.1 mm and stress drops corresponding to a coefficient of friction reduction of 0.07 to 0.11. There may be large dynamic overshoot in such cases since laboratory specimens can be poor radiators of seismic energy, but even assuming the maximum overshoot of $\Delta\sigma = 2\ (\sigma_p - \sigma_d)$, the friction coefficient reduction based on $\sigma_p - \sigma_d$ in such small slips is 0.03 to 0.05. Further, those are experiments on relatively immature surfaces. Thus the likelihood of important weakening before the range of slips shown in our data is real.

5.10 Consequences for earthquake nucleation

Earthquake nucleation on slowly loaded crustal faults has been studied extensively in the contexts of rate and state friction (Dieterich 1986; Scholz 1998; Lapusta & Rice 2003) and of linear slip weakening (Ohnaka *et al.* 1986; Campillo & Ionescu 1997; Shibazaki & Matsu'ura 1998; Ampuero & Vilotte 2002; Uenishi & Rice 2003). In those cases it is found that a localized region of initially aseismic slip develops and slowly enlarges in size over a timescale that is vastly longer than that of seismic slip. Then, over a short time compared with that of seismic slip, there is a transition from the very slow to seismic slip rates. The size of the aseismically slipping zone at that transition is called the nucleation size. Rice & Uenishi (2002) (their results are briefly summarized in Uenishi & Rice 2003) studied nucleation under slowly increasing tectonic loading, of a spatially non-uniform, locally peaked form, for a power-law slip-weakening relation like eq. (6). They assumed $\sigma_F(s) = \sigma_p - As^n$, where $A > 0$ and $n > 0$, and the law was taken in their analysis to apply near $s = 0$. They showed that if $n < 2/3$ (which is the case for us; we find $n = 0.28$), then there would be no aseismic nucleation zone like just described. Instead, dynamic rupture initiates as soon as the peak stress is reached at a single point on the fault surface.

As we have emphasized, our power law in eq. (6) should not be extended into the multimicrometre slip range over which the state transition process of rate and state friction takes place (corresponding to renewal of a long-lived contact asperity population), and thus we cannot strictly accept the prediction made by extending the law to $s = 0$. Nevertheless, the most sensible interpretation given the Rice & Uenishi (2002) result is that the aseismic to seismic transition takes place for a very small nucleation zone, possibly of a 0.1–10 m size comparable with that typically estimated by assuming that laboratory-constrained slip lengths for state evolution (0.01–0.1 mm) apply for natural faults. Certainly, an implication of their results is that stable aseismic slip is no longer possible at amounts of slip for which the power-law description of eq. (6) is valid; that is consistent with our discovery of the law as a description of states reached during dynamic instabilities.

6 CONCLUSIONS

We calculate more precise source parameters for 30 small earthquakes using strict data selection, empirical Green's function methods and an improved technique to calculate energy. We combine our results with previous studies to investigate earthquake scaling processes. We find that σ_a does increase with moment as does $\Delta\sigma$, but owing to the uncertainties in both small and large earthquake measurements, and the small size of $2\sigma_a$ relative to $\Delta\sigma$, the significance of this relationship is unclear.

Assuming that the scale dependence is real, we use the earthquake source parameters to constrain possible models of dynamic rupture. We find that the data can be modelled with a single, scale-independent frictional stress as a function of earthquake slip. The existence of such a model implies that alternative models involving a causal relationship between fault zone properties and the size of the earthquake are not the only possibility.

ACKNOWLEDGMENTS

REA is particularly grateful to H. Kanamori for many informative discussions and comments. We thank S. Ide for sending preprints of his work, and N. Beeler and an anonymous reviewer for their thoughtful reviews which significantly improved this manuscript. In addition, many people contributed to the recording of the Cajon Pass borehole data, to whom REA in particular continues to be grateful. This work was supported by NSF Award EAR 0126315 to Boston University, NSF Award EAR 0125709 to Harvard University, and by the Southern California Earthquake Center. SCEC is funded by NSF Cooperative Agreement EAR-0106924 and USGS Cooperative Agreement 02HQAG0008. The SCEC contribution number for this paper is 728.

REFERENCES

Abercrombie, R.E., 1995. Earthquake source scaling relationships from −1 to 5 M_L using seismograms recorded at 2.5 km depth, *J. geophys. Res.,* **100,** 24 015–24 036.

Abercrombie, R.E. & Leary, P., 1993. Source parameters of small earthquakes recorded at 2.5 km depth, Cajon Pass, southern California: implications for earthquake scaling, *Geophys. Res. Lett.,* **20,** 1511–1514.

Ampuero, J.-P. & Vilotte, J.-P., 2002. Insights on fault behavior from the seismic nucleation phase, *EOS, Trans. Am. geophys. Un., Fall Meeting Suppl.,* **83**(47), abstract S61E-08.

Andrews, D.J., 1976. Rupture velocity of plane strain shear cracks, *J. geophys. Res.,* **81**(32), 5679–5687.

Andrews, D.J., 1985. Dynamic plane-strain shear rupture with a slip-weakening friction law calculated by a boundary integral method, *Bull. seism. Soc. Am.,* **75**(1), 1–21.

Archuleta, R.J., 1984. A faulting model for the 1979 Imperial Valley earthquake, *J. geophys. Res.,* **89,** 4559–4585.

Beeler, N.M., Wong, T.-F. & Hickman, S.H., 2003. On the expected relationships between apparent stress, static stress drop, effective shear fracture energy and seismic efficiency, *Bull. seism. Soc. Am.,* 1381–1389.

Beroza, G.C. & Mikumo, T., 1996. Short slip duration in dynamic rupture models in the presence of heterogenous fault properties, *J. geophys. Res.,* **101,** 22 449–22 460.

Beroza, G.C. & Spudich, P., 1988. Linearized inversion for fault rupture behavior: application to the 1984 Morgan Hill, California, earthquake, *J. geophys. Res.,* **93,** 6275–6296.

Blanpied, M.L., Lockner, D.A. & Byerlee, J.D., 1995. Frictional slip of granite at hydrothermal conditions, *J. geophys. Res.,* **100,** 13 045–13 064.

Boatwright, J., 1980. A spectral theory for circular seismic sources: simple estimates of source duration, dynamic stress drop, and radiated energy, *Bull. seism. Soc. Am.,* **70,** 1–28.

Boatwright, J., Choy, G.L. & Seekins, L.C., 2002. Regional estimates of radiated seismic energy, *Bull. seism. Soc. Am.,* **92,** 1241–1255.

Bouchon, M. & Vallée, M., 2003. Observation of long supershear rupture during the $M_S = 8.1$ Kunlunshan (Tibet) earthquake, *Science,* **301,** 824–826.

Bouchon, M., Sekiguchi, H., Irikura, K. & Iwata, T., 1998. Some characteristics of the stress field of the 1995 Hyogo-ken Nanbu (Kobe) earthquake, *J. geophys. Res.,* **103,** 24 271–24 282.

Brodsky, E.E. & Kanamori, H., 2001. Elastohydrodynamic lubrication of faults, *J. geophys. Res.,* **106,** 16 357–16 374.

Brune, J.N., 1970. Tectonic stress and the spectra of seismic shear waves from earthquakes, *J. geophys. Res.,* **75,** 4997–5009.

Campillo, M. & Ionescu, I.R., 1997. Initiation of antiplane shear instability under slip dependent friction, *J. geophys. Res.,* **102,** 20 363–20 371.

Chambon, G., Schmittbuhl, J. & Corfdir, A., 2002. Laboratory gouge friction: seismic-like slip weakening and secondary rate- and state-effects, *Geophys. Res. Lett.,* **29**(10), doi:10.1029/2001GL014467.

Choy, G.L. & Boatwright, J.L., 1995. Global patterns for radiated seismic energy and apparent stress, *J. geophys. Res.,* **100,** 18 205–18 228.

Cocco, M. & Bizzarri, A., 2002. On the slip-weakening behavior of rate- and state-dependent constitutive laws, *Geophys. Res. Lett.,* **29,** doi:10.1029/2001GL013999.

Dahlen, F.A., 1977. The balance of energy in earthquake faulting, *Geophys. J. R. astr. Soc.,* **48,** 239–261.

Day, S.M., 1982. Three-dimensional finite difference simulation of fault dynamics: rectangular faults with fixed rupture velocity, *Bull. seism. Soc. Am.,* **72,** 705–727.

Dieterich, J.H., 1979. Modeling of rock friction—1 Experimental results and constitutive equations, *J. geophys. Res.,* **84,** 2161–2168.

Dieterich, J.H., 1981. Constitutive properties of faults with simulated gouge, in *Mechanical Behavior of Crustal Rocks,* American Geophysical Union Geophysical Monograph 24, pp. 103–120, eds Carter, N.L., Friedman, M., Logan, J.M. & Stearns, D.W., AGU, Washington, DC.

Dieterich, J.H., 1986. A model for nucleation of earthquake slip, in *Earthquake Source Mechanics,* American Geophysical Union Geophysical Monograph 37, Maurice Ewing Series Vol 6, pp. 37–47, eds Das, S., Boatwright, J. & Scholz, C.H., AGU, Washington, DC.

Dieterich, J.H. & Kilgore, B.D., 1994. Direct observation of frictional contacts: new insights for state-dependent properties, *Pure appl. Geophys.,* **143,** 283–302.

Dreger, D. & Helmberger, D., 1991. Source parameters of the Sierra Madre earthquake from regional and local body waves, *Geophys. Res. Lett.,* **18,** 2015–2018.

Eshelby, J.D., 1957. The determination of the elastic field of an ellipsoidal inclusion and related problems, *Proc. R. Soc. Lond.,* A, **241,** 376–396.

Favreau, P. & Archuleta, R.J., 2003. Direct seismic energy modeling and application to the 1979 Imperial Valley earthquake, *Geophys. Res. Lett.,* **30**(5), doi:10.1029/2002GL015968.

Frankel, A. & Kanamori, H., 1983. Determination of rupture duration and stress drop from earthquakes in southern California, *Bull. seism. Soc. Am.,* **73,** 1527–1551.

Gibowicz, S.J. & Kijko, A., 1994. *An Introduction to Mining Seismology,* Academic Press, San Diego, CA.

Guatteri, M. & Spudich, P., 2000. What can strong-motion data tell us about slip-weakening fault-friction laws?, *Bull. seism. Soc. Am.,* **90,** 98–116.

Guatteri, M., Spudich, P. & Beroza, G.C., 2001. Inferring rate and state friction parameters from rupture models of the 1995 Hyogo-ken Nambu (Kobe) earthquake, *J. geophys. Res.,* **106**(B11), 26 511–26 521.

Goldsby, D.L. & Tullis, T.E., 2002. Low strength during rapid frictional slip on laboratory faults in rock, *Geophys. Res., Lett.,* **29,** 4–7.

Hanks, T.C., 1977. Earthquake stress drops, ambient tectonic stresses and stresses that drive plate motions, *Pure appl. Geophys.,* **115,** 441–458.

Hardebeck, J.L. & Shearer, P.M., 2002. Using S/P amplitude ratios to improve earthquake focal mechanisms: two examples from Southern California, *EOS, Trans. Am. geophys. Un., Fall Meeting Suppl.,* **83**(47), abstract S72E-01.

Hauksson, E., 2000. Crustal structure and seismicity distribution adjacent to the Pacific and North America plate boundary in Southern California, *J. geophys. Res.,* **105,** 13 875–13 903.

Heaton, T.H., 1990. Evidence for and implications of self-healing pulses of slip in earthquake rupture, *Phys. Earth planet. Inter.,* **64,** 1–20.

Hough, S.E. & Dreger, D.S., 1995. Source parameters of the 23 April 1992 M 6.1 Joshua Tree, California, earthquake and its aftershocks; empirical Green's function analysis of GEOS and TERRAscope data, *Bull. seism. Soc. Am.,* **85,** 1576–1590.

Husseini, M.I., Jovanovich, D.B., Randall, M.J. & Freund, L.B., 1975. The fracture energy of earthquakes, *Geophys. J. R. astr. Soc.,* **43,** 367–385.

Ida, Y., 1972. Cohesive force across the tip of a longitudinal-shear crack and Griffith's specific surface energy, *J. geophys. Res.,* **77,** 3796–3805.

Ide, S., 2002. Estimation of radiated energy of finite-source earthquake models, *Bull. seism. Soc. Am.,* **92**(8), 2994–3005.

Ide, S. & Beroza, G.C., 2001. Does apparent stress vary with earthquake size, *Geophys. Res. Lett.,* **28,** 3349–3352.

Ide, S. & Takeo, M., 1997. Determination of constitutive relations of fault slip based on seismic wave analysis, *Geophys. Res. Lett.,* **102,** 27 379–27 391.

Ide, S., Beroza, G.C., Prejean, S.G. & Ellsworth, W.L., 2003. Apparent break in earthquake scaling due to path and site effects on deep borehole recordings, *J. geophys. Res.,* **108,** doi:10.1029/2001JB001617.

Imanishi, K. et al, 2004. Source parameters and rupture velocities of microearthquakes in Western Nagano, Japan, determined using stopping phases, *Bull. seism. Soc. Am.,* **94,** 1762–1780.

Ji, C., Wald, D.J. & Helmberger, D.V., 2002. Source description of the 1999 Hector Mine, California, earthquake, Part II: Complexity of slip history, *Bull. seism. Soc. Am.,* **92,** 1208–1226.

Johnson, E., 1990. On the initiation of unidirectional slip, *Geophys. J. Int.,* **101,** 125–132.

Kanamori, H. & Heaton, T.H., 2000. Microscopic and macroscopic physics of earthquakes, in *Geocomplexity and the Physics of Earthquakes,* American Geophysical Union Geophysical Monograph 120, pp. 147–163, AGU, Washington, DC.

Kanamori, H., Mori, J., Hauksson, E., Heaton, T.H., Hutton, L.K. & Jones, L.M., 1993. Determination of of earthquake energy release and M_L using TERRAscope, *Bull. seism. Soc. Am.,* **83,** 330–346.

Knopoff, L., 1958. Energy release in earthquakes, *Geophys. J.,* **1,** 44–52.

Kostrov, B.V., 1974. Seismic moment and energy in earthquakes and seismic flow of rock, *Izv. Earth Phys.,* **1,** 23–40 (from Russian).

Lachenbruch, A.H., 1980. Frictional heating, fluid pressure and the resistance to fault motion, *J. geophys. Res.,* **85,** 6097–6112.

Lapusta, N. & Rice, J.R., 2003. Nucleation and early seismic propagation of small and large events in a crustal earthquake model, *J. geophys. Res.,* **108**(B4), doi:10.1029/2001JB000793.

Ma, K.-F., Mori, J., Lee, S.-J. & Yu, S.B., 2001. Spatial and temporal distribution of slip for the 1999 Chi-Chi, Taiwan, earthquake, *Bull. seism. Soc. Am.,* **91,** 1069–1087.

Ma, K.-F., Brodsky, E.E., Mori, J., Ji, C., Song, T.-R.A. & Kanamori, H., 2003. Evidence for fault lubrication during the 1999 Chi-Chi, Taiwan, earthquake (M_W 7.6), *Geophys. Res. Lett.,* **30**(5), doi:10.1029/2002GL015380.

Madariaga, R., 1976. Dynamics of an expanding circular fault, *Bull. seism. Soc. Am.,* **66,** 639–666.

Madariaga, R., 1979. On the relation between seismic moment and stress drop in the presence of stress and strength heterogeneity, *J. geophys. Res.,* **84,** 2243–2250.

Manov, D.V., Abercrombie, R.E. & Leary, P.C., 1996. Reliable and economical high temperature deep borehole seismic recording, *Bull. seism. Soc. Am.,* **86,** 204–211.

Marone, C.J., 1998. Laboratory-derived friction laws and their application to seismic faulting, *Ann. Rev. Earth planet. Sci.,* **26,** 643–696.

Mase, C.W. & Smith, L., 1987. Effects of frictional heating on the thermal, hydrologic, and mechanical response of a fault, *J. geophys. Res.,* **92,** 6249–6272.

Mayeda, K. & Walter, W.R., 1996. Moment, energy, stress drop, and source spectra of Western United States earthquakes from regional coda envelopes, *J. geophys. Res.,* **101,** 11 195–11 208.

McGarr, A., 1999. On relating apparent stress to the stress causing earthquake slip, *J. geophys. Res.,* **104,** 3003–3011.

McGarr, A. & Fletcher, J.B., 2000. A method for mapping apparent stress and energy radiation applied to the 1994 Northridge earthquake fault zone, *Geophys. Res. Lett.,* **27,** 1953–1956.

Mikumo, T., Fukuyama, E., Olsen, K.B. & Yagi, Y., 2001. Stress-breakdown time and critical weakening slip inferred from the source time functions on earthquake faults, *EOS, Trans. Am. geophys. Un., Fall Meeting Suppl.,* **82**(47), abstract S21E-07.

Miyatake, T., 1992. Reconstruction of dynamic rupture process of an earthquake with constraints of kinematic parameters. *Geophys. Res. Lett.,* **19,** 349–352.

Mori, J., 1996. Rupture directivity and slip distribution of the M4.3 foreshock to the 1992 Joshua Tree earthquake, southern California, *Bull. seism. Soc. Am.,* **86,** 805–810.

Mori, J. & Frankel, A., 1990. Source parameters from small events associated with the 1986 North Palm Springs, California, earthquake, determined using empirical Green functions, *Bull. seism. Soc. Am.,* **80,** 278–295.

Mori, J., Abercrombie, R.E. & Kanamori, H., 2003. Stress drop and radiated energies of the Northridge aftershocks, *J. geophys. Res.,* **108,** 10.1029/200JB000474.

Nadeau, R.M. & Johnson, L.R., 1998. Seismological studies at Parkfield VI: moment release rates and estimates of source parameters for small repeating earthquakes, *Bull. seism. Soc. Am.,* **88,** 790–814.

Ohnaka, M., 1996. Nonuniformity of the constitutive law parameters for shear rupture and quasistatic nucleation to dynamic rupture: a physical model of earthquake generation processes, *Proc. Natl. Acad. Sci. USA,* **93,** 3795–3802.

Ohnaka, M.A., 2003. Constitutive scaling law and a unified comprehension for frictional slip failure, shear fracture of intact rock and earthquake rupture, *J. geophys. Res.,* **108,** doi:10.1029/2000JB000123.

Ohnaka, M., Kuwahara, Y., Yamamoto, K. & Hirasawa, T., 1986. Dynamic breakdown processes and the generating mechanism for high-frequency elastic radiation during stick-slip instabilities, in *Earthquake Source Mechanics,* American Geophysical Union Geophysical Monograph 37, Maurice Ewing Series Vol .6, pp. 13–24, eds Das, S., Boatwright, J. & Scholz, C.H., AGU, Washington, DC.

Olsen, K., Madariaga, R. & Archuleta, R., 1997. Three dimensional dynamic simulation of the 1992 Landers earthquake, *Science,* **278,** 834–838.

Olsen, K.B., Fukuyama, E. & Mikumo, T., 2001. Direct measurement of the slip weakening distance from near-fault strong-motion data?, *EOS, Trans. Am. geophys. Un., Fall Meeting Suppl.,* **82**(47), abstract S21E-08.

Orowan, E., 1960. *Mechanism of Seismic Faulting in Rock Deformation,*Geological Society of America Memoir 79, pp. 323–345, Geological Society of America, Boulder, CO.

Palmer, A.C. & Rice, J.R., 1973. The growth of slip surfaces in the progressive failure of overconsolidated clay, *Proc. R. Soc. Lond.,* A, **332,** 527–548.

Pérez-Campos, X. & Beroza, G.C., 2003. An apparent mechanism dependence of radiated seismic energy, *J. geophys. Res.,* **106,** 11 127–11 136.

Pérez-Campos, X., Singh, S.K. & Beroza, G.C., 2003. Reconciling teleseismic and regional estimates of seismic energy, *Bull. seism. Soc. Am.,* **93,** 2123–2130.

Perrin, G., Rice, J.R. & Zheng, G., 1995. Self-healing slip pulse on a frictional surface, *J. Mech. Phys. Solids,* **43,** 1461–1495.

Peyrat, S., Olsen, K. & Madariaga, R., 2001. Dynamic modeling of the 1992 Landers earthquake, *J. geophys. Res.,* **106**(B11), 26 467–26 482.

Poliakov, A.N.B., Dmowska, R. & Rice, J.R., 2002. Dynamic shear rupture interactions with fault bends and off-axis secondary faulting, *J. geophys. Res.,* **107**(B11), doi:10.1029/2001JB000572.

Prejean, S.G. & Ellsworth, W.L., 2001. Observations of earthquake source parameters and attenuation at 2 km depth in the Long Valley Caldera, Eastern California, *Bull. seism. Soc. Am.,* **91,** 165–177.

Rice, J.R., 1980. The mechanics of earthquake rupture, in *Physics of the Earth's Interior,* pp. 555–649, eds Dziewonski, A.M. & Boschi, E., Italian Physical Society/North Holland Publishing Company, Amsterdam.

Rice, J.R., 1996. Low-stress faulting: Strong but brittle faults with local stress concentrations, *EOS, Trans. Am. geophys. Un., Fall Meeting Suppl.,* **77**(46), F471.

Rice, J.R., 2000. Fracture energy of earthquakes and slip-weakening rupture parameters, *EOS, Trans. Am. geophys. Un., Fall Meeting Suppl.,* **81**(48), F1227.

Rice, J.R. & Ben-Zion, Y., 1996. Slip complexity in earthquake fault models, *Proc. Natl. Acad. Sci. USA,* **93,** 3811–3818.

Rice, J.R. & Uenishi, K., 2002. Slip development and instability on a heterogeneously loaded fault with power-law slip-weakening, *EOS, Trans. Am. geophys. Un., Fall Meeting Suppl.,* **83**(47), abstract S61E-06.

Rice, J.R., Sammis, C.G. & Parsons, R., 2004. Off-fault secondary failure induced by a dynamic slip-pulse, *Bull. seism. Soc. Am.,* **95,** 109–134, doi:10.1785/0120030166.

Richardson, E. & Jordan, T.H., 2002. Seismicity in deep gold mines of South Africa: implication for tectonic earthquakes, *Bull. seism. Soc. Am.,* **92,** 1766–1782.

Rudnicki, J.W. & Wu, M., 1995. Mechanics of dip-slip faulting in an elastic half-space, *J. geophys Res.,* **100**(B11), 22 173–22 186.

Ruina, A., 1983. Slip instability and state variable friction laws, *J. geophys. Res.,* **88,** 10 359–10 370.

Sammis, G.C. & Rice, J.R., 2001. Repeating earthquakes as low-stress-drop events at a border between locked and creeping fault patches, *Bull. seism. Soc. Am.,* **91,** 532–537.

Sato, T. & Hirasawa, T., 1973. Body wave spectra from propagating shear cracks, *J. Phys. Earth,* **21,** 415–431.

Scholz, C.H., 1998. Earthquakes and friction laws, *Nature,* **391,** 37–42.

Shibazaki, B. & Matsu'ura, M., 1998. Transition process from nucleation to high-speed rupture propagation: scaling from stick-slip experiments to natural earthquakes, *Geophys. J. Int.,* **132,** 14–30.

Shipton, Z.K. & Evans, J.P., 2003. Analysis of exhumed fault zones and evidence for deformation at the base of the seismogenic zone, *Geophys. Res. Abstr.,* **5**, 12459.

Sibson, R.H., 1973. Interactions between temperature and pore-fluid pressure during earthquake faulting and a mechanism for partial or total stress relief, *Nature,* **243**(126), 66–68.

Sibson, R.H., 1975. Generation of pseudotachylyte by ancient seismic faulting, *Geophys. J. R. astr. Soc.,* **43,** 775–794.

Singh, S.K. & Ordaz, M., 1994. Seismic energy release in Mexican subduction zone earthquakes, *Bull. seism. Soc. Am.,* **84,** 1533–1550.

Spray, J.G., 1993. Viscosity determinations of some frictionally generated silicate melts; implications for fault zone rheology at high strain rates, *J. geophys. Res.,* **98,** 8053–8068.

Spray, J.G., 1995. Pseudotachylyte controversy; fact or friction?, *Geology,* **23,** 1119–1122.

Stork, A.L. & Ito, H., 2004. Source parameter scaling for small earthquakes observed at the western Nagano 800 m-deep borehole, central Japan, *Bull. seism. Soc. Am.,* **94,** 1781–1796.

Tomic, J., Abercrombie, R.E. & do Nascimento, A., 2003. Source parameters of reservoir-induced small earthquakes: can we resolve rupture velocity?, *EOS, Trans. Am. geophys. Un., Fall Meeting Suppl.,* **84**(46), abstract S42C-0178.

Tse, S.T. & Rice, J.R., 1986. Crustal earthquake instability in relation to the depth variation of frictional slip properties, *J. geophys. Res.,* **91,** 9452–9472.

Tullis, T.E. & Weeks, J.D., 1986. Constitutive behavior and stability of frictional sliding in granite, *Pure appl. Geophys.,* **124,** 383–414.

Uenishi, K. & Rice, J.R., 2003. Universal nucleation length for slip-weakening rupture instability under non-uniform fault loading, *J. geophys. Res.,* **108**(B1), doi:10.1029/2001JB001681.

Venkataraman, A. & Kanamori, H., 2004. Observational constraints on the fracture energy of subduction zone earthquakes, *J. geophys. Res.,* **109,** doi:10.1029/2003JB002549.

Venkataraman, A., Mori, J., Kanamori, H. & Zhu, L., 2000. Fine structure of the rupture zone of the April 26 and 27, 1997, Northridge aftershocks, *J. geophys. Res.,* **105,** 19 085–19 093.

Venkataraman, A., Rivera, L. & Kanamori, H., 2002. Radiated energy from the 16 October 1999 Hector Mine earthquake: regional and teleseismic estimates, *Bull. seism. Soc. Am.,* **92,** 1256–1265.

Wald, D.J., 1995. A preliminary dislocation model for the 1995 Kobe (Hyogo-ken Nanbu), Japan, earthquake determined from strong motion and teleseismic waveforms, *Seism. Res. Lett.,* **66,** 22–28.

Wald, D.J. & Heaton, T.H., 1994. Spatial and temporal distribution of slip for the 1992 Landers, California, earthquake, *Bull. seism. Soc. Am.,* **84,** 668–691.

Wald, D.J., Helmberger, D.V. & Heaton, T.H., 1991. Rupture model of the 1989 Loma Prieta earthquake from the inversion of strong-motion and broadband teleseismic data, *Bull. seism. Soc. Am.,* **81,** 1540–1572.

Wald, D.J., Heaton, T.H. & Hudnut, K.W., 1996. The slip history of the 1994 Northridge, California, earthquake determined from strong-motion, teleseismic, GPS, and leveling data, *Bull. seism. Soc. Am.,* **86**(1, Part B Suppl.),49–70.

Wong, T.-F., 1982. Shear fracture energy of Westerly granite from post-failure behavior, *J. geophys. Res.,* **87,** 990–1000.

Wong, T.-F., 1986. On the normal stress dependence of the shear fracture energy, in *Earthquake Source Mechanics,* American Geophysical Union Geophysical Monograph 37, Maurice Ewing Series Vol. 6, pp. 1–11, eds Das, S., Boatwright, J. & Scholz, C.H., AGU, Washington, DC.

Wyss, M., 1970. Stress estimates for South American shallow and deep earthquakes, *J. geophys. Res.,* **75,** 1529–1544.

Yamada, T., Mori, J., Kawakata, H., Ogasawara, H., Ide, S. & Tanbo, S., 2002. Rupture velocities of small earthquakes ($0 \leq M \leq 1.5$) in a South African gold mine: constraints on fracture energy, *EOS, Trans. Am. geophys. Un., Fall Meeting Suppl.,* **83**(47), abstract S72B-1143.